Science of the Total Environment 984 (2025) 179453

Contents lists available at ScienceDirect

Science of the Total Environment

journal homepage: www.elsevier.com/locate/scitotenv

Short to long term space-time prediction of rain-induced landslides under uncertainty

Alessandro C. Mondini [a], Fausto Guzzetti [b,*], Massimo Melillo [c], Antonio Pievatolo [d]

[a] Consiglio Nazionale delle Ricerche, Istituto di Matematica Applicata e Tecnologie Informatiche "Enrico Magenes", via de Marini 6, Genova I-16149, Italy
[b] Consiglio Nazionale delle Ricerche, Istituto di Matematica Applicata e Tecnologie Informatiche "Enrico Magenes", formerly Istituto di Ricerca per la Protezione Idrogeologica, via de Marini 6, Genova I-16149, Italy
[c] Consiglio Nazionale delle Ricerche, Istituto di Ricerca per la Protezione Idrogeologica, via della Madonna Alta 126, Perugia I-06128, Italy
[d] Consiglio Nazionale delle Ricerche, Istituto di Matematica Applicata e Tecnologie Informatiche "Enrico Magenes", via Bassini 15, Milano I-20133, Italy

HIGHLIGHTS

- Transient rainfall history controls location and time of rain-induced landslides in Italy
- Long term, multi-decadal analysis of landslide occurrence probability in Italy
- Synoptic-scale landslide hazard as a combination of probabilistic prediction models

GRAPHICAL ABSTRACT

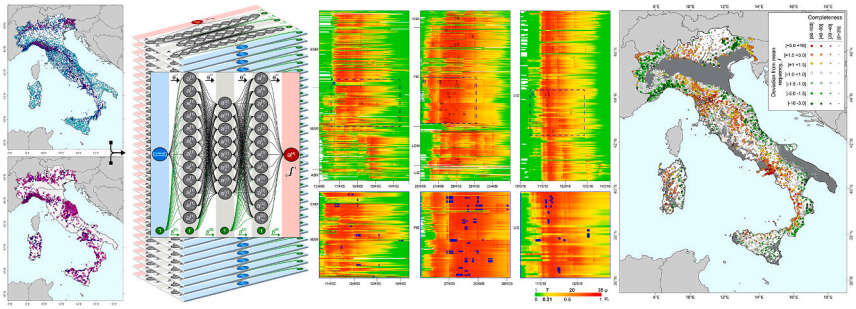

ARTICLE INFO

Editor: Demetrio Antonio Zema

Keywords:
Landslide
Forecast
Prediction
Deep network
Hazard
Poisson binomial distribution

ABSTRACT

Rainfall is the primary natural trigger for landslides, and their threat is expected to rise as the climate warms. To mitigate the consequences of rain-induced landslides, predicting where and when landslides may occur is crucial. We propose a probabilistic modelling framework for synoptic-scale, short-term (hours to days) to long-term (years to decades) space-time prediction of rain-induced landslides. The framework employs a Poisson binomial distribution for the number of successes in a set of Bernoulli trials, each representing a landslide prediction with its own success probability. Our predictors are 35 deep networks that predict landslides occurrence based on rainfall data and information on past landslides. We tested the framework in Italy using hourly rainfall data from 4031 rain gauges and historical landslide records between 2002 and 2022. Results show that hourly rainfall history provides sufficient information to predict the location and timing of landslides without the need for rainfall thresholds or to define event-based rainfall metrics. Applying the forecasting system to 184,080 h between 1 January 2002 and 31 December 2022 we generated a unique, multi-decadal representation of the expected long-term occurrence probability of rain-induced landslides in Italy, which was not otherwise available from landslide catalogues, inventory maps or susceptibility zoning. We expect the modelling framework to enhance landslide early warning systems and to support long-term landslide adaptation and risk reduction strategies. The approach opens the possibility to consider landslide hazard as a combination of independent

* Corresponding author.
E-mail addresses: alessandrocesare.mondini@cnr.it (A.C. Mondini), fausto.guzzetti@cnr.it (F. Guzzetti), massimo.melillo@cnr.it (M. Melillo), antonio.pievatolo@cnr.it (A. Pievatolo).

https://doi.org/10.1016/j.scitotenv.2025.179453
Received 11 February 2025; Received in revised form 12 April 2025; Accepted 14 April 2025
Available online 25 May 2025

prediction models of landslide occurrence with associated uncertainty, thus changing the existing paradigm for landslide hazard assessment.

1. Introduction

Rainfall is the primary natural trigger for landslides (Wieczorek, 1996), and the threat of rain-induced landslides is expected to increase due to the warming climate (Gariano and Guzzetti, 2016; Pánek, 2019; Emberson et al., 2020; Dahal et al., 2024a) and the expansion of population and developments into vulnerable terrain (Ozturk et al., 2022; Jakob, 2022). In order to reduce the environmental, social, and economic costs of landslides, the anticipation of rain-induced landslides is becoming increasingly important for environmental management, urban and land planning, and civil protection (European Commission Joint Research Centre, 2017; Piciullo et al., 2018; Guzzetti et al., 2020). Despite significant improvements over the last five decades, the ability to jointly predict over large areas when and where rain-induced landslides will occur over periods ranging from a few hours to several years – the timescale of interest for early warning, environmental management, and adaptation strategies – remains limited (Guzzetti, 2021b). There are many reasons for this, including the complexity and variability of the prediction problem, exacerbated by the lack of systematic data on landslide occurrence. Unlike for other hazards, regional, continental or global systems for the systematic detection of landslides (Stanley et al., 2021) are lacking. This hinders the ability to verify hypotheses about the physical causes of failure and to evaluate the performance of the prediction models. Here, we propose a general approach to the synoptic-scale, short term (hours to days) to long term (years to decades) prediction of rain-induced landslides.

The paper is structured as follows. First, we describe the problem of the spatio-temporal prediction of landslides, and how it is addressed in the landslide literature (Section 2). Next, we present a theoretical modelling framework for synoptic-scale probabilistic prediction of rain-induced landslides at different temporal scales, from hours to decades (Section 3). We then present the study area, Italy (Section 4), the rainfall data and the landslide information available to us to test the theoretical framework (Section 5). Next, we describe the modelling framework (Sections 6), present the results of our modelling efforts (Section 7), and discuss the results and their specific and general characteristics (Section 8). We conclude summarising the main findings and lessons learned (Section 9).

2. Background and motivation

2.1. Temporal prediction

In the literature, predicting "when" or "how often" landslides are expected to occur in an area is done using two general approaches, depending on the timescale of the problem. Short-term prediction – in the following, "landslide forecast", typically from hours to a few days – is made using empirical rainfall thresholds or mechanistic numerical models. Empirical rainfall thresholds are established using heuristic or statistical approaches and typically define the minimum amount of rainfall variables (*e.g.*, rainfall duration, cumulated rainfall, rainfall intensity and their variations and normalizations (Guzzetti et al., 2007)) that, when reached or exceeded (Reichenbach et al., 1998), can lead to landslide occurrence (*e.g.*, Glade et al., 2000; Crosta and Frattini, 2000; Aleotti, 2004; Guzzetti et al., 2007, 2008; Saito et al., 2010; Ko and Lo, 2018; Segoni et al., 2018; Guzzetti et al., 2024; Mirus et al., 2025). Mechanistic – also known as "physically based" – models simulate numerically the dynamic conditions of slopes forced by rainfall. This is achieved by more or less complex, geographically distributed, coupled hydrological–slope instability models that consider the dynamically changing balance of forces acting in a slope affected by rainfall mainly through infiltration (*e.g.*, Montgomery and Dietrich, 1994; Van Asch et al., 1996; Borga et al., 1998; Burton and Bathurst, 1998; Baum et al., 2008; Lanni et al., 2013; Formetta et al., 2014; Anagnostopoulos et al., 2015; Reid et al., 2015; Formetta et al., 2016; Alvioli and Baum, 2016; Bout et al., 2018).

Early rainfall thresholds and mechanistic models for landslide forecasting date back to the mid-1980s, when the first geographical landslide early warning systems (LEWS) were tested in Hong Kong (Chan et al., 2003; Choi and Cheung, 2013; Wong et al., 2014; Kong et al., 2020) and in the San Francisco Bay Area, USA (Keefer et al., 1987; Wilson, 2012), and mechanistic models were experimented in Japan and the USA (Okimura and Ichikawa, 1985; Dietrich et al., 1993; Montgomery and Dietrich, 1994). Since then, dozens operational geographical LEWS have been implemented (Piciullo et al., 2018; Guzzetti et al., 2020) and numerous mechanistic, hydrologic–slope instability models have been proposed and tested in different geological, climatic, and environmental settings.

This large body of work reveals limitations of the rainfall thresholds and mechanistic models for landslide forecasting. Empirical rainfall thresholds rely on temporally-aggregated measures of precipitation (Guzzetti et al., 2008; Segoni et al., 2014, 2015) and most commonly do not consider the full set of the triggering and non-triggering (Crozier, 1999; Peres and Cancelliere, 2021) rainfall conditions, hampering the possibility to estimate the probability of landslide occurrence *versus* the probability of non-occurrence (Peres and Cancelliere, 2021; Mondini et al., 2023). Mechanistic models are limited mainly to small catchments due to their challenging requirements for mechanical and hydrological slope properties, which can have ample geographical variations and are difficult and costly to obtain over large areas (Lim et al., 2024; Piciullo et al., 2018; van den Bout et al., 2021; Monte et al., 2024).

Long-term predictions, instead, focus on estimating "how often" landslides occur in periods from years to decades. Estimates are typically obtained calculating the frequency of past landslides, or of landslide triggering events (*e.g.*, rainstorms) in an area, which are then projected in the future assuming stationarity of the landslide triggering processes, an assumption whose validity is difficult to prove, or disprove. The expected, long-term frequency of landslides, or of rainfall events that can result in landslides, is obtained chiefly through statistical or probabilistic modelling of time series of known (past) landslides obtained from archive inventories or catalogues (*e.g.*, Lips and Wieczorek, 1990; Coe et al., 2000; Crovelli and Coe, 2009; Guzzetti et al., 2003; Rossi et al., 2010; Witt et al., 2010; Staley et al., 2020), or from high-quality multi-temporal landslide maps (Guzzetti et al., 2012) obtained though more or less systematic interpretation and analysis of aerial and satellite imagery (Lombardo et al., 2020; Jones et al., 2021; Lim et al., 2024). The approach suffers from various problems, including (i) the inevitable incompleteness of the landslide time series obtained from archive sources, especially in remote areas, in large areas, and in the more distant past, resulting in biased, underestimated or noisy frequencies, (ii) the availability, temporal spacing, and quality of the aerial and satellite imagery used to prepare multi-temporal inventories (Guzzetti et al., 2012), which limits their preparation to a few decades, (iii) the low geographical resolution of the prediction, dependent on the numerosity – including completeness – of the events in the historical record, and (iv) the fact that the conditions, including meteorological, climate, geological, and environmental conditions that control landslide occurrence may have changed over long periods, affecting the rate of landslide occurrence – *i.e.*, the expected frequency of landslide occurrence (Dahal et al., 2024b).

2.2. Spatial prediction

The spatial prediction of landslides consists in predicting "where" landslides are expected to occur in an area. In the literature, this involves assessing landslide "susceptibility" (Brabb, 1984, 1985), the probability of landslides occurring in an area given the local terrain and environmental conditions. Initiated in the mid-1970s and early 1980s in Europe with the work of Hubert (1976) in France, Neuland (1976) in Germany, and Carrara (1983) in Italy, susceptibility modelling and zonation has evolved over the last four decades from a direct, qualitative, mostly heuristic effort based on geomorphological mapping (Hansen, 1984), to an indirect, quantitative, data-driven classification effort that exploits known or inferred functional (statistical) relationships between a set of terrain and environmental variables and the known presence or absence of (past) landslides (Reichenbach et al., 2018).

Inspection of the vast literature reveals that for modelling and zoning landslide susceptibility, investigators have employed a wide range of data-driven methods (Michie et al., 1994), including frequentist, Bayesian, and machine learning classification methods (Guzzetti et al., 1999; Chung and Fabbri, 1999; Van Westen et al., 2006; van Westen et al., 2008; Reichenbach et al., 2018) applied to a large number of study areas, at different geographical scales, and in different and diverse geological, physiographic, and climatic settings (Reichenbach et al., 2018; Dahal and Lombardo, 2025). This vast body of literature has identified several limitations with susceptibility modelling, the most important of which for our scope is that the spatial probability of landslide occurrence obtained is – by definition (Reichenbach et al., 2018; Guzzetti, 2021b) – time-invariant, and the time frame or period for the validity of the prediction is not explicitly or implicitly stated, or is arbitrarily set to correspond to the period during which the terrain and environmental variables (*e.g.*, morphology, geology, hydrology, soils, land use, land cover) used to construct the classification model have not changed, or are not expected to change in the future (Guzzetti et al., 2005; Reichenbach et al., 2018); another assumption that is difficult to prove, or disprove.

2.3. Joint spatial and temporal prediction

Attempts to jointly predict "when" and "where" rain-induced landslides may occur in an area exist and are getting increasing interest in the literature. Based on the time frame of the prediction, the attempts can be classified into short-term forecasts and long-term predictions.

Short-term spatio-temporal forecasts are at the core of geographical LEWS for landslide surveillance and early warning with regional to nearly global coverage (Piciullo et al., 2018; Guzzetti et al., 2020). In the systems, the "spatial" (geographical) component of the forecast is given by, and dependent on, the geographical distribution, coverage, and spatial resolution of the rainfall information obtained from *e.g.*, rain gauges, weather radars, satellite estimates or their combinations, whereas the "temporal" component is obtained from rainfall measurements modelled through empirical or statistical thresholds, mechanistic models, or their combination (Guzzetti et al., 2020).

Alternative approaches have been tested in recent years. Mondini et al. (2023) proposed a synoptic-scale, spatio-temporal forecast of rain-induced landslides in Italy, an area of $\approx$ 302,000 km^2. Using granular information on rainfall events that did or did not result in known landslides in a nearly two-decade period, the authors built a large ensemble of simple deep learning models that they used to forecast, in space and time, the occurrence, or lack of occurrence, of rain-induced landslides in Italy from February 2002 to December 2020. Adopting the simplifying assumption of a binary susceptibility, with $S = 1$ where landslides can occur and $S = 0$ elsewhere, the forecasts were made only where rain-induced landslides where deemed possible *i.e.*, where $S = 1$. The work proved that accurate, synoptic scale, spatio-temporal forecast of rain-induced landslides can be done effectively in very large, diverse and complex areas using only hourly rainfall measurements.

Nocentini et al. (2024) used a machine learning approach based on a random forest algorithm to determine the spatio-temporal occurrence probability of weather-related landslides caused by two meteorological events in June 2011 and May 2013, in a 2800 km^2 area in southern Norway, for which landslide inventories – *i.e.*, accurate spatial and temporal landslide information – were available. To train, test, and validate the random forest algorithm, the authors used a mix of dynamic (*i.e.*, time-varying) meteorological and weather variables (*e.g.*, cumulated daily rainfall and snowmelt, and their seasonal variability) and static (*i.e.*, time-invariant) variables describing the morphological and environmental setting of their study area.

Similarly, Lim et al. (2024) used time-varying dynamic variables derived from satellite daily precipitation estimates from the Climate Hazards Centre Infrared Precipitation with Stations – CHIRPS (Funk et al., 2015) over the four-decade period 1981–2021, static morphological and environmental variables, and spatial and temporal landslide information obtained from event landslide inventories, to perform landslide forecast for early warning in selected areas of Vietnam. The authors divided their study areas into slope units (Alvioli et al., 2016), and used a fully connected neural network informed by the static variables to obtain a susceptibility zonation of their study areas *i.e.*, the spatial component of the forecast. In parallel, they used a Gated Recurrent Unit neural network informed by rainfall variables derived from precipitations time series to obtain the temporal component of the forecast. They then used a second fully connected neural network to combine the spatial and the temporal components into a space-time forecast of landslide occurrence. The two later papers (Nocentini et al., 2024; Lim et al., 2024) have in common the attempt to predict the time of landslide occurrence directly from the precipitation time series, without using derivative or lumped rainfall measures, or rainfall thresholds. Potentially, this is a major advantage over studies that relay on thresholds or lumped measures of the rainfall trigger over pre-defined periods (Mondini et al., 2023).

Long-term spatial and temporal predictions typically exploit static – *i.e.*, time invariant in the modelling period – morphological and environmental variables and landslide information from multi-temporal landslide inventory maps or archives.

Lombardo et al. (2020) used a Bayesian modelling framework to predict the spatial and temporal occurrence of weather-triggered landslides in a 79 km^2 area in Umbria, central Italy. The authors assumed that individual landslides in their study area from before 1941 to 2014 were the result of a point process that they modelled as a Log-Gaussian Cox process (Møller et al., 1998; Basu and Dassios, 2002; Diggle et al., 2013) with a stochastic Poisson component to model the number of landslides, a proxy for susceptibility, and a stochastic Gaussian component to model the spatial distribution of the environmental conditions controlling landslide occurrence. Moreno et al. (2024) used Generalized Additive Mixed Models to integrate precipitation measurements at different temporal scales, static ground conditions and seasonal effects, and information on $>$ 1000 precipitation-induced landslides from 2000 to 2020 in South Tyrol, Italy, to develop a predictive space-time model of shallow landslide occurrence in a 7400 km^2 study area in the central Alps, combining spatially distributed, static terrain and environmental data with two dynamic, daily precipitation measures before the day of the landslides.

Fang et al. (2024) used annual landslide data between 2004 and 2018 in Taiwan obtained from optical satellite imagery with static environmental and dynamic meteorological variables to construct a spatio-temporal model of landslide occurrence, assuming that landslide susceptibility obeys a binomial distribution and landslide size a log-Gaussian distribution. They then combined the predictions using a generalized additive model approach to obtain a spatio-temporal prediction of landslide hazard. Dahal et al. (2024a) proposed a similar model for the long-term, space-time prediction of landslide hazard *i.e.*, "where" landslides are expected to occur measured by susceptibility, the

expected landslide "threat" measured by landslide "intensity", and the expected landslide frequency or return period. Working in Nepal, the authors used daily satellite precipitation estimates obtained from CHIRPS (Funk et al., 2015), time-invariant morphological and environmental information from different sources, and landslide information from the inventory compiled by Jones et al. (2021) showing rain-triggered landslides in central-eastern Nepal from 1988 to 2018, to inform a deep-learning model that estimated a Bernoulli distribution used to describe susceptibility, and an extended Generalized Pareto Distribution (Papastathopoulos and Tawn, 2013) used to model landslide intensity, the probability that the landslide size or density in each mapping unit exceeds a given value. Assuming stationarity over the modelling period, the extreme-value model for the rainfall driver allowed to compute long-term return levels for each slope unit, providing the temporal component of the hazard model.

These and other similar studies required detailed geomorphological and environmental data, as well as accurate multi-temporal information on landslides, in areas ranging in size from tens to thousands of square kilometres, with the study areas subdivided into slope units (Alvioli et al., 2016). With current detection and mapping capabilities, multi-temporal landslide information for a very large area – tens to hundreds of thousands of square kilometres (*e.g.*, for the whole of Italy) – and updating this information after each landslide-triggering rainfall event – is not currently performed operationally, limiting the possibility of using statistical modelling techniques for space-time landslide prediction. Also, the studies did not consider possible spatial-temporal clustering of landslides (*e.g.*, the "heritage" of new landslides on older one (Samia et al., 2017), they assumed the stationarity of the landslide initiation processes and that the morphological and environmental settings have not changed (statistically) in the study areas in the considered period, something difficult to prove over large areas and for long periods of time (Guzzetti et al., 2005, 2009; Dahal et al., 2024a).

2.4. Motivation

There is growing evidence that the footprint and abundance of landslides triggered by rainfall mimic the spatio-temporal pattern of precipitation in different climatic, geological, seismic, and environmental settings around the world (*e.g.*, Benz and Blum, 2019; Bessette-Kirton et al., 2019; Handwerger et al., 2019; Emberson et al., 2022; Perkins et al., 2024), and certainly in Italy (*e.g.*, Crosta, 1998; Bandis et al., 1999; Luino, 1999; Guzzetti et al., 2004; Roccati et al., 2018; Donnini et al., 2023; Santangelo et al., 2023; Berti et al., 2025). Supported by this empirical evidence, and building on recent results that showed that rain-induced landslides can be predicted in space and time using rainfall measurements (Mondini et al., 2023; Lim et al., 2024), we propose a probabilistic modelling framework for the synoptic-scale, short to long-term spatio-temporal prediction of rain-induced landslides.

3. Theoretical framework

Our modelling framework is based on the assumption that the dynamically changing footprint of a rainfall event over a period of hours to a few days controls the onset, location, and timing of the rain-induced landslides where landslides can occur (Mondini et al., 2023) *i.e.*, where susceptibility is not negligible (Marchesini et al., 2014). Then, recognizing the intrinsic aleatory variability of the landslide triggering processes, and in an attempt to address the epistemic uncertainty inherent in the landslide and the rainfall data and, most importantly, in our understanding of the landslide triggering processes – a particularly severe problem at the synoptic scale and for large and diverse areas (Marzocchi and Jordan, 2014; Mondini et al., 2023) – we adopt a probabilistic approach for the short-term, space-time forecasting of rain-induced landslides.

To cope with uncertainty – including possible biases and gaps in the landslide and rainfall data – we prepare an ensemble of models each simulating a Bernoulli trial. We consider the outcomes of the Bernoulli trials as independent, and to combine them we use the Poisson binomial distribution (PBD) (Hoeffding, 1956; Wang, 1993; Biscarri et al., 2018), the discrete probability distribution of a sum of independent Bernoulli trials. Specifically, the probability mass function (PMF) of the PBD defines the probability of a specific number of successes in a set of n conditionally independent Bernoulli trials, each with a success probability $p_i \in [0:1]$, with $i = 1 \ldots n$:

$$PMF = P(X = k) = \sum_{A \in F_k} \prod_{i \in A} p_i \prod_{j \in A^c} \left(1 - p_j\right), \tag{1}$$

where, k are the successful (*i.e.*, "yes") trials out of n possible trials, A is any subset of F_k, the set of all subsets of k integers that can be selected from 1, 2, ..., n, and i and j are counters in sets A and A^c, respectively. Conveniently, the PBD admits mean, $\mu = \sum_{i=1}^{n} p_i$ and variance, $\sigma^2 = \sum_{i=1}^{n} (1 - p_i) p_i$, which we take to be the expected values of the prediction and its uncertainty.

In this framework, $p_i = P_i(L|R,S)$ represents the probability that a landslide, L will occur given the rainfall history, R in an area characterised by susceptibility, $S \in [0:1]$. Assuming that susceptibility, S does not change dynamically with the rainfall history (Reichenbach et al., 2018; Guzzetti, 2021a), and adopting the simplifying assumption that $S = 1$ where landslides can occur and $S = 0$ elsewhere (Mondini et al., 2023), the outcome of the i-th Bernoulli trial becomes $p_i = P_i(L|R) \times c$, where $c = 1$ where landslides can occur and $c = 0$ elsewhere. Following Mondini et al. (2023), we focus on areas where landslides can occur and we estimate the set of p_i's with our ensemble of prediction models. Any model capable of providing a landslide prediction in probabilistic terms, with an associated measure of uncertainty, will do the work. Here, we use an ensemble $\mathscr{M}$ of n fully connected deep neural networks (Abadi et al., 2015) prepared using bagging (Breiman, 1996) to account for data uncertainty, and informed by a set of rainfall variables to describe the rainfall history and information on the occurrence, or non occurrence of known landslides.

We consider $\mathscr{M}$ as a group of n independent forecasters, each independently interpreting the same rainfall history measured at a rain gauge. Each forecaster answers the question "*given the hourly rainfall history, how likely is a landslide to occur?*" and she provides p_i that we interpret as the probability of the "success" outcome of a Bernoulli trial $p_i(landslide = yes \mid r)$, where i is the i-th deep network and r is the rainfall history at the given rain gauge ($R = r$). Each forecaster provides a different probability, p_i. The probability of agreement among the forecasters is captured by PBD, and we take the mean, μ of the PDB (*i.e.*, the expected number of forecasters that agree on landslide occurrence) as our prediction of possible landslide occurrence, and its variance, σ^2 as a measure of its uncertainty.

4. Study area

Located in southern Europe, Italy covers an area of $\approx$ 302,000 km^2 from the Alps to the central Mediterranean, between 35° and 47° N and 6° and 19° E (Fig. 1). Italy's physiography is diverse and is characterised by two main mountain ranges, the Alps in the north, which run from west to east and separate Italy from central Europe, and the Apennines, which form the backbone of the Italian peninsula. The climate is warm-summer humid continental (Dfb) to cold (ET) in the north, depending on elevation, and hot-summer Mediterranean (Csa), humid subtropical (Cfa), and cold semi-arid (BSk) in the centre and the south, depending on elevation and latitude (Beck et al., 2023). Mean annual precipitation (MAP) – mostly rain and subordinately snow – ranges from $<$ 300 mm to $>$ 2000 mm, with the western coasts wetter than the eastern. Due to geology, morphology, meteorology, and climate, landslides of various types are common in Italy (Trigila et al., 2010), with almost 635,000 known landslides as of February 2025 (Istituto Superiore per la Protezione e la Ricerca Ambientale, 2025). Excluding the large plains, this

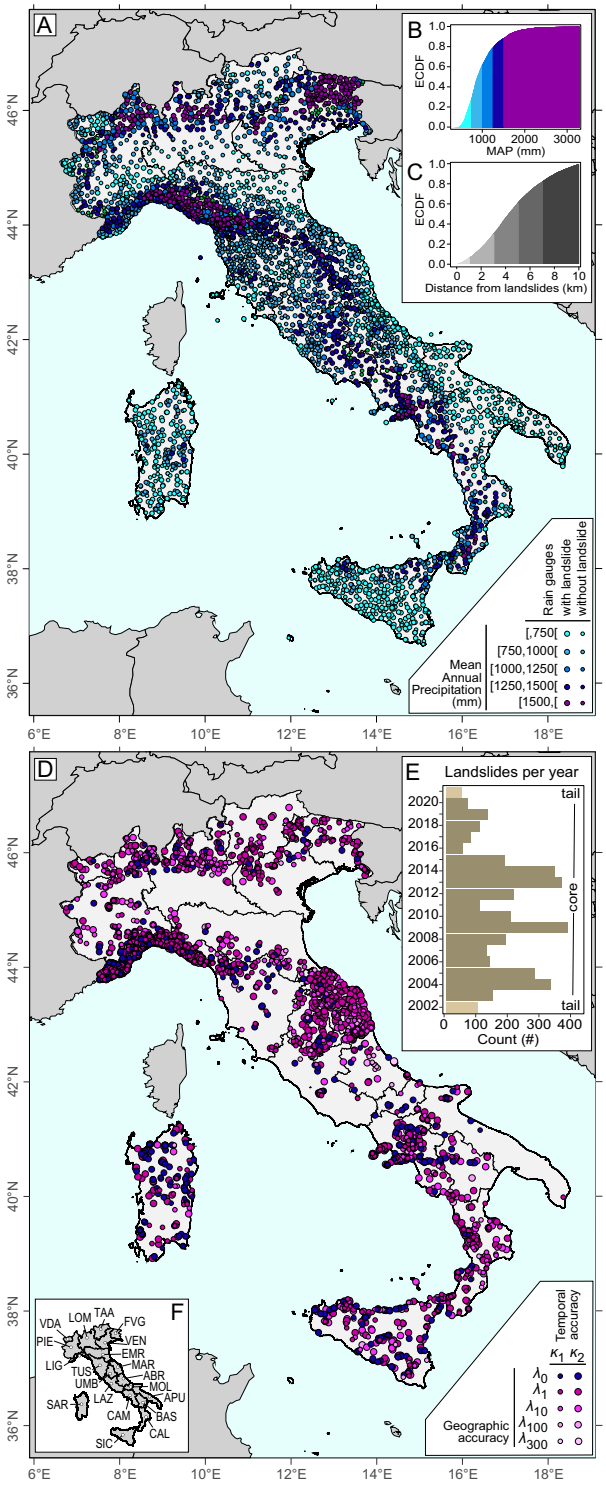

(caption on next column)

Fig. 1. Rainfall and landslide information. (A) Location of 4031 rain gauges represented by dots coloured based on the rain gauge mean annual precipitation (MAP), in 5 classes. Large dots show 2365 gauges associated with landslides used to train, validate, and test the ensemble of 35 deep network models, $\mathscr{M}$. Small dots show 1666 rain gauges not associated with landslides. (B) Empirical cumulative distribution function, ECDF of the MAP of all the rain gauges, coloured in the same 5 classes of MAP as in (A). (C) ECDF of the planimetric distance between the rain gauges and up to the 3 nearest landslides within a distance of 10 km. (D) Location of 3722 landslides obtained from the ITALICA catalogue (Peruccacci et al., 2023). Landslides are shown by dots of two sizes depending on temporal accuracy, κ and coloured according on their geographical accuracy, λ in 5 classes: λ_0, very high accuracy, exact landslide location; λ_1, high accuracy, $\lambda < 1$ km^2; λ_{10}, medium accuracy, $1 \leq \lambda < 10$ km^2; λ_{100}, low accuracy, $10 \leq \lambda < 100$ km^2; λ_{300}, very low accuracy, $100 \leq \lambda < 300$ km^2. Small dots indicate 2542 landslides with high temporal accuracy, κ_1 when the time – minute to hour – of the landslide was known, and large dots indicate 1180 landslides with low temporal accuracy, κ_2 when the part of the day was known *e.g.*, early morning, late morning, midday, early afternoon, late afternoon, early night, night. (E) Annual count of landslides. Landslides from 2003 to 2020 (dark bars) were used to train, validate and test $\mathscr{M}$ and to independently evaluate the performance of the models ensemble. Landslides in 2002 and 2021 (light bars) were used to independently evaluate the performance of $\mathscr{M}$. (F) Regions index map. ABR, Abruzzo; APU, Apulia; BAS, Basilicata; CAL, Calabria; CAM, Campania; EMR, Emilia-Romagna; FVG, Friuli-Venezia Giulia; LAZ, Lazio; LIG, Liguria; LOM, Lombardy; MAR, Marche; MOL, Molise; PIE, Piedmont; SAR, Sardinia; SIC. Sicily; TAA, Trentino-Alto Adige; TUS, Tuscany; UMB, Umbria; VDA, Valle d'Aosta; VEN, Veneto.

corresponds to an average density of > 3 landslides per km^2, the highest known in Europe. Rainfall is the main trigger of landslides, and single rainfall events or short rainfall periods can trigger hundreds to tens of thousands of landslides (*e.g.*, Crosta, 1998; Bandis et al., 1999; Luino, 1999; Guzzetti et al., 2004; Pizziolo et al., 2015; Roccati et al., 2018; Santangelo et al., 2023; Donnini et al., 2023; Berti et al., 2025). The social and economic consequences of landslides are high in Italy (Rossi et al., 2019), with 1070 dead and missing persons, 1443 injured people, and 138,743 evacuated and homeless between 1974 and 2023 (Bianchi and Salvati, 2025).

Italy's geographical extent and location in the Mediterranean, its diverse physiographic, climatic, and meteorological settings, the abundance of landslides, and the availability of an extensive catalogue of recent landslides and of rainfall records covering the same period, make it an ideal area to test our hypotheses and modelling framework.

5. Materials

To test our assumptions and the modelling framework presented above we use hourly rainfall measurements from 4031 rain gauges, and information on the location and time of occurrence of ≈ 3700 rain-induced landslides over the 21-year period 2002–2022, in Italy.

5.1. Rainfall data

We obtain hourly rainfall measurements spanning the period from 1 January 2002, at 00:00 to 31 December 2022, at 23:59 (local time), covering a total of 7670 days or 184,080 h. The hourly measurements were taken by a network of 4031 automatically recording rain gauges (Fig. 1A), resulting in ≈ 3.88×10^8 hourly records, including ≈ 2.49×10^7 records with precipitation *i.e.*, with hourly rainfall measurements $\geq$ 0.2 mm, which represent our rainfall modelling set {R}. With gauge spacing ranging from 0.03 km to ≈ 10.00 km (average ≈ 4.49 km), the network has an average of one gauge per ≈ 75 km^2 *i.e.*, one gauge every ≈ 8.7 km × 8.7 km (Fig. 1B), a globally high gauge density (Kidd et al., 2017), which we consider adequate to capture the rainfall conditions that can trigger landslides in the different physiographic settings in Italy (Peruccacci et al., 2017; Mondini et al., 2023).

There are temporal and geographical biases in the rainfall data, with the completeness of records increasing with time, and the density of rain gauges varying from region to region, and over time. Overall, the highest gauge density is found in Liguria, with one gauge every 26 km^2, followed by Tuscany, with one gauge every 34 km^2, and Marche, with one gauge every 39 km^2, whereas the lowest gauge density is found in Veneto, with one gauge every 164 km^2, followed by Lombardy, with one gauge every 145 km^2, and Basilicata, with one gauge every 134 km^2 (Table 1).

Table 1
Name, code, area extent, number of rain gauges, average area covered per rain gauge, and number of landslides in each region, and for Italy. Regions are loosely listed from NW to S.

Region	Code	Area km^2	Rain gauges #	Area per gauge km^2/#	Landslides #
Valle d'Aosta	VDA	3260	53	61.5	26
Piedmont	PIE	25,388	304	83.5	172
Lombardy	LOM	23,863	163	146.4	172
Trentino-Alto Adige	TAA	13,605	118	115.3	54
Veneto	VEN	18,406	112	164.3	82
Friuli-Venezia Giulia	FVG	7863	164	47.9	64
Liguria	LIG	5416	205	26.4	1219
Emilia-Romagna	EMR	22,453	246	91.3	56
Tuscany	TUS	22,986	674	34.1	115
Umbria	UMB	8465	97	87.3	147
Marche	MAR	9401	242	38.8	588
Lazio	LAZ	17,233	197	87.5	24
Abruzzo	ABR	10,830	199	54.4	41
Molise	MOL	4460	47	94.9	13
Campania	CAM	13,671	172	79.5	249
Basilicata	BAS	10,074	75	134.3	44
Apulia	PUG	19,540	221	88.4	48
Calabria	CAL	15,221	145	105.0	175
Sardinia	SAR	24,100	233	103.4	175
Sicily	SIC	25,832	364	71.0	258
Italy	ITA	302,067	4031	74.9	3722

5.2. Landslide information

We use landslide information taken from the ITAlian rainfall-triggered LandslIdes CAtalogue – ITALICA (Peruccacci et al., 2023) (Fig. 1D). Compiled through an expert analysis of newspapers, blogs, online resources, and technical and event reports, ITALICA is an archive inventory (Guzzetti et al., 2012) that lists information on the location and time or period of occurrence of mostly shallow landslides in Italy between January 1996 and December 2021, including first-time (*i.e.*, new) failures, first-time failures within pre-existing landslides, and partial or total reactivations of pre-existing landslides. Due to the sources of information used to compile ITALICA, the catalogue has some geographical bias, with more information in the Liguria and subordinately in the Marche regions compared to other geographical areas. Considering the paucity of accurate information on the time and location of landslides in Italy, we use all the available landslide information in ITALICA. We note that the degree of completeness of ITALICA is unknown, but the catalogue lists an unknown percentage of all the rainfall induced landslides that have occurred in Italy between 2002 and 2021, most of which were not reported or had insufficient information to be included in the catalogue (Peruccacci et al., 2023).

ITALICA assigns to each landslide a geographical accuracy, λ in five classes, and a temporal accuracy, κ in three classes (Peruccacci et al., 2023). We select the subset of landslides between January 2002 and December 2021 (20 years) for which (i) the location is known exactly or within one km^2 (*i.e.*, within a radius of 0.6 km from the landslide), and (ii) the exact time (minute to hour) or the part of the day (*i.e.*, early or late morning, midday, early or late afternoon, evening, night) is known or inferred (Peruccacci et al., 2023). The selection resulted in 3722 landslides (Table 1), including 2542 slope failures for which the failure time is known within one hour (68.3 %), 440 within two hours (11.8 %), 249 within three hours (6.7 %), and 491 within five hours (13.2 %). Of the 3722 selected landslides, 697 (18.7 %) have a very high (exact location) and 1851 (49.7 %) a high (within one km^2) geographical accuracy in the catalogue (Fig. 1D).

6. Modelling framework

To model the possible occurrence of rainfall induced landslides in Italy we implement the framework shown in Fig. 2.

6.1. Rain gauges – Landslides association

We predict the possible occurrence of rainfall induced landslides where rainfall is measured *i.e.*, at the location of the rain gauges (Mondini et al., 2023). To account for the uncertainty inherent in the spatially and temporally dynamic rainfall fields that may have caused the known landslides, and the temporal and spatial accuracy of the available landslide information (Fig. 1D), we assign each landslide to up to the three nearest rain gauges within a planimetric distance of 10 km from the landslide. We find that of all the rain gauges, 2367 (58.7 %) are associated with one or more landslides (Fig. 1C) *i.e.*, are within a distance of up to 10 km from one or more of the 3722 selected landslides. Many, but not all, of the remaining 1666 rain gauges are located in alluvial plains or flat intra-mountain basins where landslide susceptibility is negligible and landslides are not expected (Marchesini et al., 2014) (Fig. 1A).

We also consider the temporal accuracy, κ of the landslides. For landslides with high temporal accuracy in the catalogue *i.e.*, when the time of the slope failure is known exactly or within one hour, we assign the landslide ($l = 1$) to the same hour in the corresponding rainfall record, or records if the landslide has been assigned to two or three rain gauges. For landslides for which the temporal accuracy is intermediate *i.e.*, when the failure time is known within a period from two to five hours depending on the time of day, we consider the length of the accuracy period (*i.e.*, two, three or five hours). Since ITALICA assigns the time of the landslide to the end of the last hour of the accuracy period (Peruccacci et al., 2023), for landslides with a temporal accuracy of two hours, we assign the landslide to the same hour and to the preceding hour in the corresponding rainfall records (Fig. 3A). Similarly, for landslides with a temporal accuracy of three (or five) hours, we assign

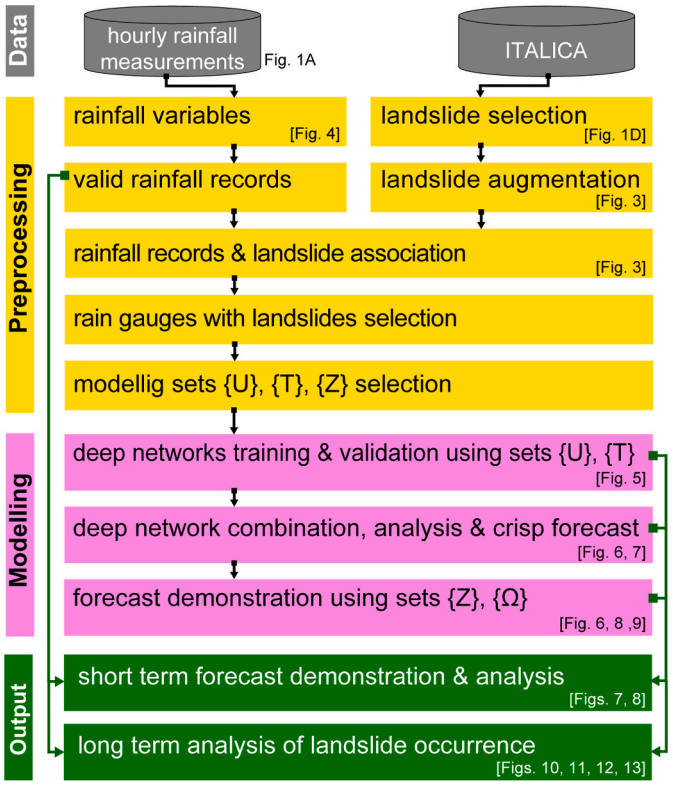

Fig. 2. Modelling framework for synoptic-scale, short to long-term spatio-temporal prediction of rain-induced landslides, under uncertainty. The chart shows (i) input rainfall and landslide data used for the study (grey), (ii) data preprocessing (yellow), (iii) modelling *i.e.*, deep network training, combination, and short term demonstration, and (iv) short term demonstration and long term analysis of landslide occurrence and hazard assessment (green).

the landslide to the same hour and to the preceding two (or four) hours in the corresponding rainfall records (Fig. 3C,D). For example, for a landslide reported at 15:00 h with a temporal accuracy of three hours, we set $l = 1$ for the 15:00, 14:00, and 13:00 h in the rainfall record(s) (Fig. 3C). We set $l = 0$ for all other hourly records.

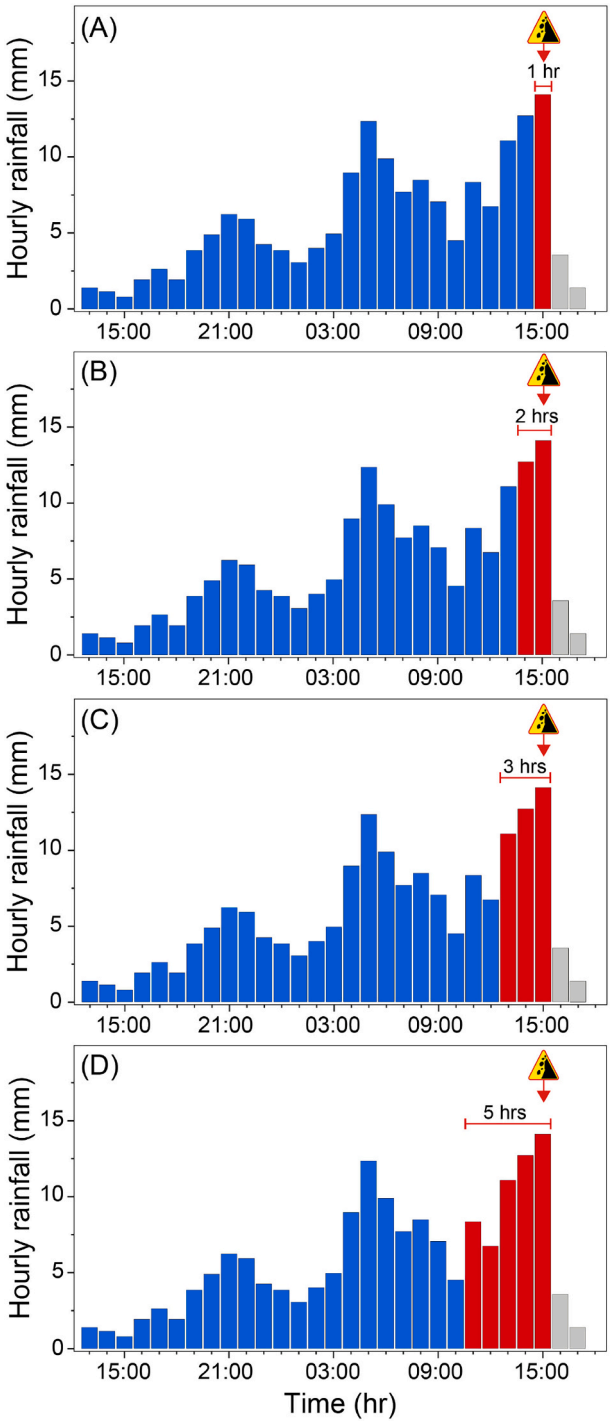

Fig. 3. Association of landslides and hourly rainfall records. Red bars show hourly rainfall (in mm) in the accuracy period. Blue bars show hourly rainfall prior to the accuracy period, κ. Grey bars show hourly rainfall after the hour of the landslide, not used for modelling. (A) Landslide with high temporal accuracy assigned to the same hour in the rainfall record. (B) Landslide with two-hour temporal accuracy assigned to the same hour and to the previous hour. (C) Landslide with three-hour temporal accuracy assigned to the same hour and to the two previous hours. (D) Landslide with five-hour temporal accuracy assigned to the same hour and to the four previous hours.

6.2. Rainfall variables

For each hourly record in the rainfall modelling set, {R} we compute 74 variables representing the rainfall history that has, or has not resulted in known landslides at or near each rain gauge. The variables measure the cumulative rainfall (in mm) in the reference t_0 hour (EH), in the preceding periods from 1 to 72 h (TR_1, TR_2, …, TR_{71}, TR_{72}, where the subscripts indicate the length of the accumulation period), and in the period that considers the rainfall accumulation from $t_0 + 73$ to $t_0 + 792$ hours (30 day antecedent period, $TR_{73\text{-}792}$) (Fig. 4). We exclude rainfall records with < 0.2 mm of rain (the measuring accuracy of most rain gauges in the network) in the preceding 72 h, as we consider this a lower limit for the triggering of rainfall induced landslides. To account for climate conditions, we add to each record in set {R} the MAP of the rain gauge, which is known to discriminate rainfall conditions leading to rainfall induced landslides in Italy (Peruccacci et al., 2017). Hence, for each hourly record in {R} we have 75 explanatory variables describing the rainfall history, and one binary variable describing the occurrence ($l = 1$) or non occurrence ($l = 0$) of known rain-induced landslides.

6.3. Rainfall modelling sets

For demonstration and independent evaluation of the prediction modelling framework (Fig. 2), we first form subset {Z} by randomly selecting from {R} 3 % of all the hourly records per year between 2003 and 2020, and all the records with ($l = 1$) and without ($l = 0$) landslides in the years 2002 and 2021. Next, using a classic Train–Validation–Test data segmentation scheme (Kuhn and Johnson, 2013), we split the remaining records into subsets {U} for training, {V} for validation, and {T} for testing. We obtain {T} by randomly selecting 5 % of the hourly records with and without an associated landslide from {R} - {Z}. From the remaining records we form {U} with 90 % of the hourly records, and {V} with 10 % of the records with landslides. To account for the much larger number of records without ($l = 0$) than with ($l = 1$) landslides, we test different imbalance ratios and obtain best results with 5 : 1 ratio as a compromise allowing adequate sampling of the records lacking landslides without increasing excessively the relevance of the true and negative values in the evaluation metrics. We recognise that different ratios would give slightly different results. We repeat the random selection of {U} and {V} multiple times to construct subsets $\{U_i\}$ and $\{V_i\}$, with i from 1 to 35, which we use to obtain the ensemble $\mathcal{M}$ of fully connected deep networks, by bagging (Breiman, 1996).

6.4. Deep networks structure, training, and validation

We construct the ensemble $\mathcal{M}$ with 35 fully connected deep networks with the same geometry (Fig. 5) with one input layer to ingest the explanatory variables, here represented by a single neuron, three hidden layers with 12, 8, and 12 neurons, and one output layer with a single neuron that gives the expected landslide occurrence probability, $p_i(1|\mathbf{x}, \boldsymbol{\theta}_i, \boldsymbol{\beta}_i)$ given the explanatory variables, 1104 weights, Θ_i and 33 biases, β_i connecting the neurons obtained in the model training and validation phase, using the $\{U_i\}$ and $\{V_i\}$ subsets (Haykin, 2009; Aggarwal, 2018). We select this network geometry after testing various alternatives, including 4 × 4, 4 × 8, 8 × 8, 8 × 8 × 8 hidden layer geometries, and various combinations of explanatory variables, including TR_1, …, TR_{72}, $TR_{73\text{-}792}$ (73 variables), EH, TR_1, …, TR_{72}, $TR_{73\text{-}792}$ (74 variables), TR_1, …, TR_{72}, $TR_{73\text{-}792}$, MAP (74 variables), EH, TR_1, …, TR_{72}, $TR_{73\text{-}792}$, MAP (75 variables), TR_1, …, TR_{48}, $TR_{49\text{-}72}$, $TR_{73\text{-}792}$ (50 variables), EH, TR_1, …, TR_{24}, $TR_{25\text{-}72}$, $TR_{73\text{-}792}$ (26 variables), TR_1, …, TR_{24}, $TR_{25\text{-}72}$, $TR_{73\text{-}792}$, MAP (26 variables), EH, TR_1, …, TR_{24}, $TR_{25\text{-}72}$, $TR_{73\text{-}792}$, MAP (28 variables), TR_1, …, TR_{24}, $TR_{25\text{-}72}$, $TR_{73\text{-}792}$ (26 variables), EH, TR_1, …, TR_{24}, $TR_{25\text{-}72}$, $TR_{73\text{-}792}$ (27 variables), TR_1, …, TR_{24}, $TR_{25\text{-}72}$, $TR_{73\text{-}792}$, MAP (27 variables), and EH, TR_1, …, TR_{24}, $TR_{25\text{-}72}$, $TR_{73\text{-}792}$, MAP (28 variables).

Assuming an *a priori* probability threshold to separate the rainfall

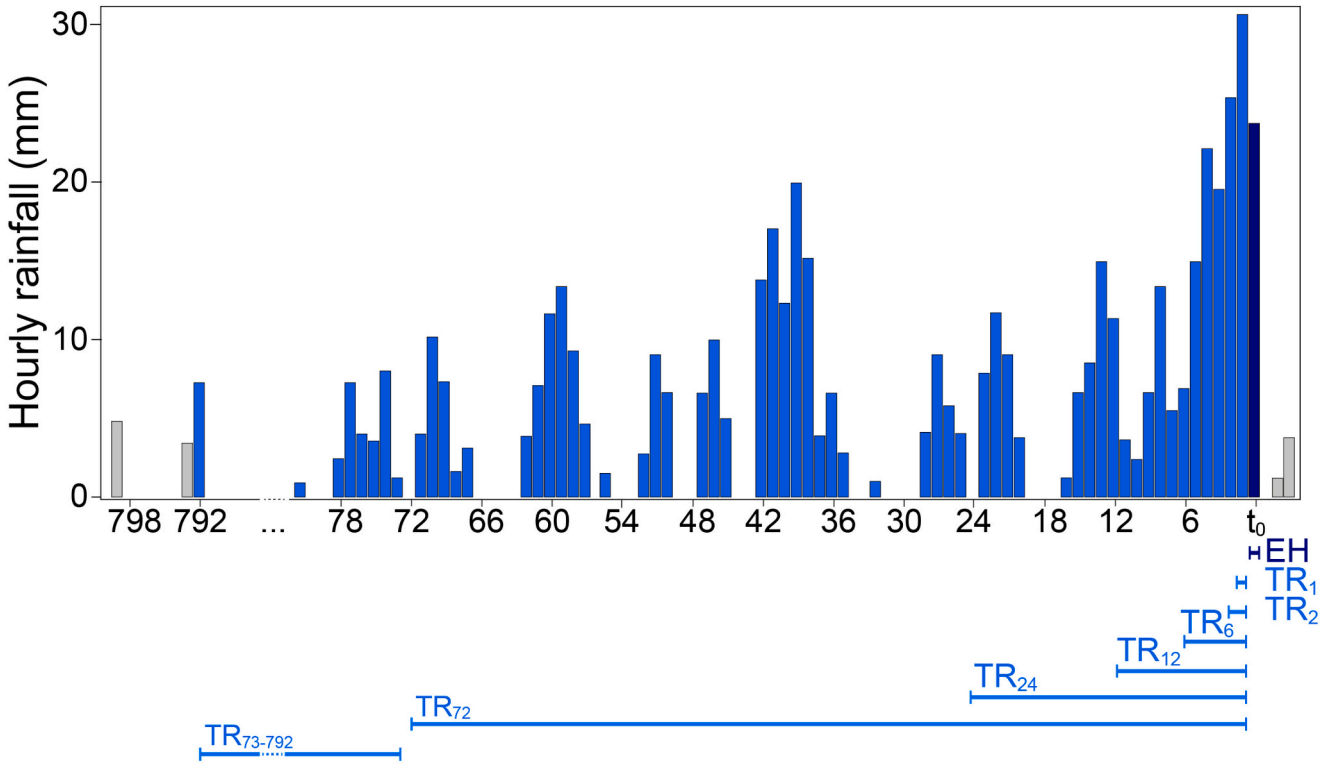

Fig. 4. Calculation of the rainfall variables used as input to the deep network models, in $\mathscr{M}$ (Fig. 5). Bar chart shows an example of an hourly rainfall record. Dark blue bar is the t_0, reference hour, and EH is the total hourly rainfall in the reference hour. Blue bars show hourly rainfall prior to the t_0 reference hour, from 1 to 792 h. Grey bars show hourly rainfall not included in the 793 h considered period. Horizontal light blue lines below the bar chart show accumulation periods for variables EH, TR_1, TR_2, TR_6, TR_{12}, TR_{24}, TR_{72}, and $TR_{73\text{-}792}$.

events predicted as having, $p_i > 0.5$ from those predicted as not having, $p_i \leq 0.5$ landslides, we obtain accuracies from 0.869 to 0.898 for both the training and the validation steps. The similar model performance for the $\{T_i\}$ and the $\{V_i\}$ subsets for all i suggests the lack of overfitting and a good generalisation capacity of the single models, $\mathscr{M}_i$ (Aggarwal, 2018). Occasionally, the model validation loss curve was slightly lower than the corresponding training curve, possibly due to an excessive regularisation (see supplementary materials Fig. 1). Fine tuning of the network geometry and the related parameters (see supplementary materials Table 1) might lead to better training of single models, $\mathscr{M}_i$. We test each network using ROC curves applied to {T} obtaining $0.907 \leq A_{ROC} \leq 0.911$, and trade off values between the True Positive Rate (*i.e.*, the sensitivity, TP/(TP+FN)) and the False Positive Rate (*i.e.*, FP/(FP+TN)) in the range 0.116 to 0.549.

6.5. Models combination

We consider the 35 deep networks in $\mathscr{M}$ as 35 independent forecasters who separately interpret the same rainfall history measured at each rain gauge. Each deep network models (*i.e.*, each forecaster answers) the question "*given the measured hourly rainfall history, how likely is a landslide to occur?*" to obtain p_i, where $p_i \in [0, 1]$, which we interpret as the probability of the "success" outcome of a Bernoulli trial $p_i(landslide = yes \mid rain)$, where i is the i-th deep network and *rain* is the rainfall history at the given rain gauge, r. Each model (*i.e.*, each forecaster) gives a different probability, p_i. Following section 3, the number of successes in the collection of n independent Bernoulli trials with probabilities p_1, p_2, ..., p_n obeys the Poisson binomial distribution (PBD) (Hoeffding, 1956; Wang, 1993; Biscarri et al., 2018)) whose PMF is given by eq. 1. We take the mean of the PBD, μ, or its scaled value $\mu_n = \mu/35$, as the expected forecast of landslide occurrence, and the variance, σ^2 as a measure of its uncertainty.

7. Results

7.1. Forecasts evaluation

We measure and demonstrate the performance of the forecast system using the hourly records of the independent subset {Z} not used in the Train-Validation-Test phase. Overall, from 2002 to 2021, the system proved capable of forecasting the hourly (short-term) probability of landslide occurrence with an high accuracy measured by a Brier score, $BS = 0.042$ (Brier, 1950) and an $A_{ROC} = 0.896$, slightly lower than the values obtained in the deep networks Train-Validation-Test phase, $0.908 \leq A_{ROC} \leq 0.912$ (Fig. 6).

We perform separate geographical, temporal, and climate evaluations of the hourly forecasts. Fig. 7A shows the geographical distribution of the 4031 rain gauges where the forecasts were verified. The symbols colour, from green to yellow to orange to red, show μ and $\mu_n = \mu/35$ the hourly predicted probability of landslide occurrence, and the size of the symbol the variance, σ^2. Yellow indicates $\mu = 7$, $\mu_n = \mu/35 = 0.2$, the best trade-off in the ROC curve obtained for {Z} (Fig. 6B), which we use to transform the probabilistic forecast into a "crisp" forecast. Visual inspection of the map does not reveal obvious geographical biases in the hourly forecasts. This is confirmed by Brier scores calculated for different topographic provinces in Italy (Guzzetti and Reichenbach, 1994) – namely, the Alpine Mountain System (AL, $BS = 0.042$), the Alpine-Apennine Transition Zone (AA, $BS = 0.056$), the Apennine Mountain System (AP, $BS = 0.045$), the Thyrrenian Bordeland (TB, $BS = 0.034$), the Adriatic Bordeland (AB, $BS = 0.027$), Sicily (SI, $BS = 0.041$), and Sardinia (SA, $BS = 0.040$) – that are all similar and very small (Fig. 7B), an evidence of the good and consistent performance of the forecast system in the different provinces.

For the temporal evaluation, we analyse the hourly forecasts grouped by year and by season. Fig. 7C shows the results per year with $0.028 \leq$

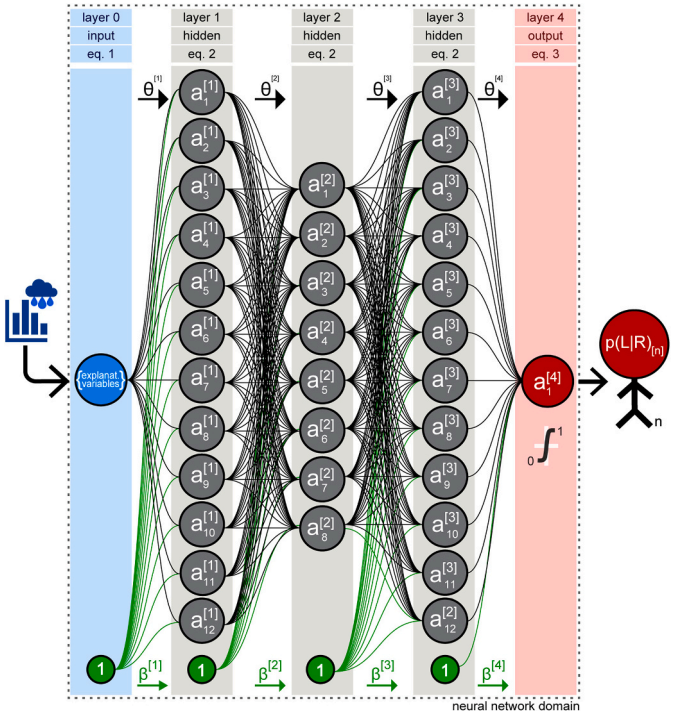

Fig. 5. Deep network geometry. In the network domain, circles are neurons arranged in five layers. In the input layer 0, the light blue circle comprises 75 explanatory variables, EH, TR_1, TR_2, …, TR_{71}, TR_{72}, $TR_{73\text{-}792}$, MAP (mean annual precipitation). In the hidden layers 1, 2 & 3, grey circles represent the 32 neurons, each activated by a *tanh* function, and green circles are symbolic variables to introduce biases. In the output layer 4, red circle represents the single output neuron activated by a sigmoid function, *h*. a_n^k is neuron *n* in the *k* layer, β_n^k in $\boldsymbol{\beta}^{[k]}$ is the bias added to the *n* neuron in the *k* layer, and $\boldsymbol{\theta}_n^k$ in $\boldsymbol{\theta}^{[k]}$ is the weight array of the neurons in the *k* - 1 layer in the *n* neuron of the layer *k*. eq. 1, explanatory variables; eq. 2, $a^n = tanh\left(\boldsymbol{\theta}^{[1,2,3]T}\boldsymbol{x} + \boldsymbol{\beta}^{[k]}\right)$; eq. 3, $a^n = h\left(\boldsymbol{\theta}^{[4]T}\mathbf{a}^2 + \boldsymbol{\beta}^{[3]}\right)$. *T* stands for transpose.

$BS \leq 0.057$, all similar and very small scores ($\mu = 0.041$, $\sigma^2 = 0.007$). Similarly, Fig. 7D shows the results obtained by grouping the hourly forecasts in two seasonal periods; June to September (dry season) and October to May (wet season). The Brier scores for the two seasonal periods are $BS_{dry} = 0.030$ and $BS_{wet} = 0.046$. We further analyse the hourly forecasts for different mean annual precipitation (MAP). Fig. 7E shows the results considering MAP in five classes. The Brier scores are all similar and very small ($\mu = 0.040$, $\sigma^2 = 0.008$).

We conclude that the system proved capable to forecast the short-term (hourly) probability of landslide occurrence with high accuracies and no apparent geographical or temporal biases, despite inhomogeneities in the rainfall and the landslide information (Fig. 1).

7.2. Operational landslide forecasting

From an operational perspective, the evaluation of the forecast system confirms that in a large and diverse landslide-prone landscape forced by rainfall, the rainfall history contains the necessary information to forecast the occurrence probability of rain-induced landslides (Mondini et al., 2023) without the need to establish rainfall thresholds (Guzzetti et al., 2008; Gonzalez, 2024), and to decide *a priori* on a period over which to consider rainfall to divide the precipitation history into events that trigger or do not trigger landslides (Melillo et al., 2018). The result has implications for landslide surveillance and early warning (European Commission Joint Research Centre, 2017; Piciullo et al., 2018; Guzzetti et al., 2020), and it can contribute to improve regional to national operational landslide forecasting.

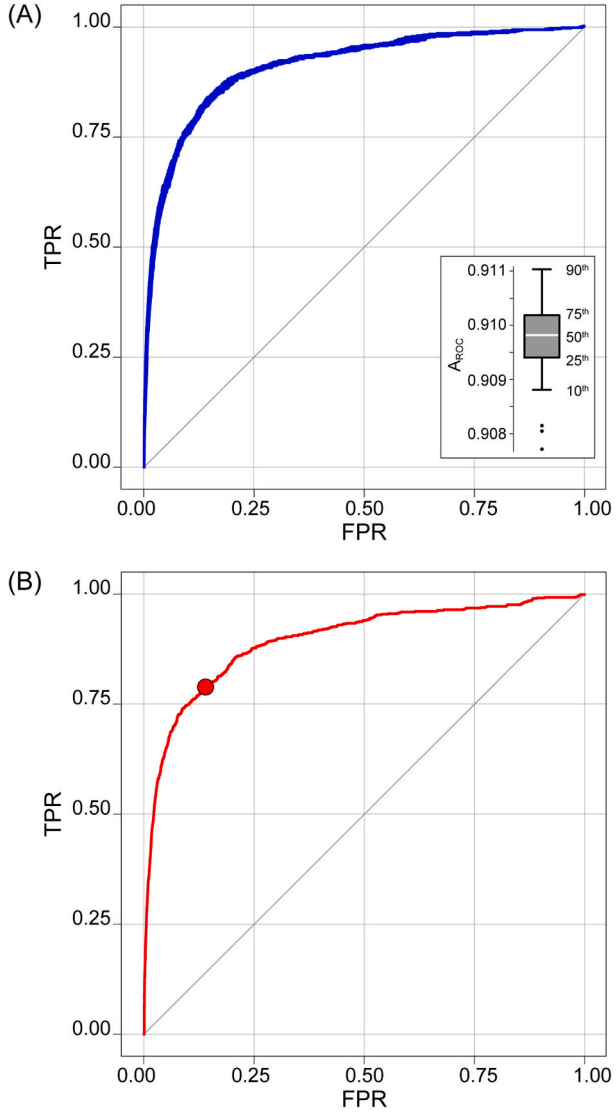

Fig. 6. Deep networks performance. (A) Performance of the deep networks during the Test and Validation phases. Plot shows 35 ROC curves for 35 deep network models prepared for subset {T}. Box plot shows the variability of A_{ROC}, in the range 0.907–0.911, median = 0.909. (B) Performance of the forecast demonstration. Plot shows the ROC curve for subset {Z}, with $A_{ROC} = 0.896$. Red dot marks best trade-off between false positive rate, FPR and true positive rate, TPR. In the two plots, specificity is *TN*/(*TN*+*FP*) and sensitivity is *TP*/(*TP*+*FN*). See also supplementary materials Table 2.

We demonstrate how the forecasts can be used operationally at the regional scale using one of the rainfall events that have caused rain-induced landslides in Italy from 2003 to 2020 namely, the event that hit northwestern Italy in mid March 2018 causing widespread landsliding (Figs. 8A and 11C). A cold front moving from the western Atlantic through the Bay of Biscay to the Ligurian Sea in the western Mediterranean crossed the region of Liguria from west to east in about two days, bringing heavy and widespread rainfall from the afternoon of 10 March to the afternoon of 12 March 2018. Rain began around 18:00 on 10 March and intensified in the early hours of 11 March over the central and western parts of the region, peaking around noon. Rainfall rate intensified in the early hours of 10 March moving from west to east. Then, rainfall moved across the eastern part of Liguria around 18:00 and stopped in the afternoon of 12 March. Landslides were first reported in western Liguria on 11 March at 00:00, and then were numerous in central Liguria before 12:00. The last landslides were reported north of

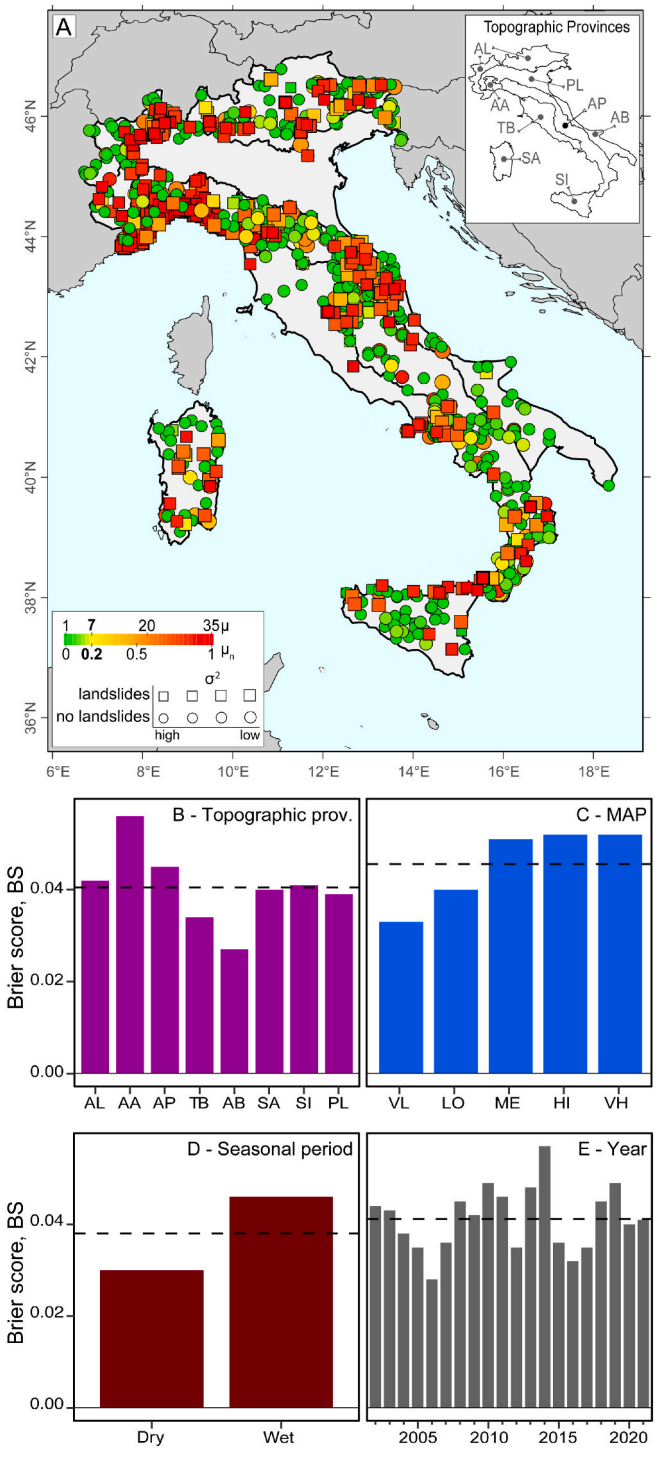

Fig. 7. Evaluation of the forecast system using independent subset {Z}. (A) Map of hourly landslide forecasts. For display purpose, an equal number of rain gauges with (circle) and without (square) known landslides are shown. Symbol colour, from green to yellow to red, shows $\mu_n = \mu/35$. Size of symbols shows forecasts variance, σ^2 with larger symbols representing smaller variance and smaller symbols larger variance. Inset map shows topographic provinces of Guzzetti and Reichenbach (1994). (B) Brier scores (Brier, 1950) for different topographic provinces (Guzzetti and Reichenbach, 1994): AL, Alpine Mountain System, $BS = 0.042$, $n = 16{,}957$ hourly records; AA, Alpine-Apennine Transition Zone, $BS = 0.056$, $n = 3695$ hourly records; AP, Apennine Mountain System, $BS = 0.045$, $n = 30{,}943$ hourly records; TB, Thyrrenian Bordeland, $BS = 0.034$, $n = 6750$ hourly records; AD, Adriatic Bordeland, $BS = 0.027$, $n = 5387$ hourly records; SA, Sardinia, $BS = 0.040$, $n = 3153$ hourly records. SI, Sicily, $BS = 0.041$, $n = 3694$ hourly records; PL, North Italian Plain, $BS = 0.039$, $n = 2955$ hourly records. (C) Brier scores in five MAP classes: VL, very low [0–800] mm, $BS = 0.033$, $n = 19{,}048$ hourly records; LO, low [800–1200] mm, $BS = 0.040$, $n = 29{,}666$ hourly records; ME, medium]1200–1600] mm, $BS = 0.051$, $n = 14{,}949$ hourly records; HI, high]1600–2000] mm, $BS = 0.052$, $n = 6831$ hourly records; VH, very high]> 2000] mm, $BS = 0.048$, $n = 3040$ hourly records. (D) Brier scores for two seasonal periods: dry season, June to September, $BS = 0.030$, $n = 19{,}280$ hourly records; wet season, October to May, $BS = 0.046$, $n = 54{,}254$ hourly records. (E) Brier scores per year.

(caption on next column)

Genoa on 13 March 15:00. Fig. 8A shows, in 6-h intervals, the cumulative rainfall from 18:00 on 10 March to 18:00 on 14 March 2018, in Liguria and in the neighbouring areas. In the Figure, the 16 maps describe the dynamic evolution of the rainfall forcing during the 96-h observation period. Fig. 8B shows the corresponding probabilistic forecasts of possible landslide occurrence, $\mu_n = \mu/35$, for the same period. In the maps, the cumulated rainfall and the landslide forecasts are shown every 6 h, but rainfall measurements and landslide forecasts are available every hour. The information presented in the forecast maps, and their dynamic evolution can be used operationally for landslide surveillance and early warning, as well as for timely advice and initiation of risk reduction measures by mandated agencies or organizations (Keefer et al., 1987; Wilson, 2012; Calvello and Piciullo, 2016; Guzzetti et al., 2020).

Fig. 9 exemplifies the complex "transformation" performed by the system – *i.e.*, the ensemble $\mathscr{M}$ of $n = 35$ independent forecasters and their combination through PBD – of the rainfall history, r at each rain gauge into hourly forecasts in the observation period. Inspection of the plots shows that our 35 forecasters – *i.e.*, the deep networks – responded quickly and with high agreement to the rainfall input, a period when most of the landslides occurred. After the rainfall peak, the median value of the forecasts decreased and the models showed relatively less agreement. Overall, the vast majority of landslides (> 95 %) occurred with $\mu > 7$, >73 % for $\mu > 25^{th}$ percentile, and >49 % for $\mu > 50^{th}$ percentile.

Inspection of Fig. 8B shows that the predicted probability of landslide occurrence remains high (orange to red, $\mu > 17$) for several hours after the end of the rainfall event (Fig. 8A). This is coherent with the empirical evidence that landslides can occur hours to days after the end of a rainfall event. In an operational environment, expert users of LEWS can consider the dynamic conditions and adapt their information and risk reduction actions based on information provided by the system (Fig. 9) and additional, external information not provided by the system (Guzzetti et al., 2020).

7.3. Long term landslide occurrence probability

We apply the forecast system to the full set {R} of available hourly rainfall measurements, and we obtain a diachronic spatio-temporal representation of the probabilistic fingerprint of the rainfall conditions that have, and could have led to rain-induced landslides in Italy from 2002 to 2022. This is represented by the "forecast mat" in Fig. 10 (with enlargements in Fig. 11) where colours show the predicted hourly probability of landslide occurrence and yellow indicates $\mu = 7$, $\mu_n = \mu/35 = 0.2$.

Of the 184,080 h shown in the "forecast mat" (Figs. 10), 81.19 % has $\mu_n < 0.2$ – *i.e.*, fewer than 7 out of 35 forecasters (deep network models) agreed on predicting landslide occurrence. This is not surprising, as rain-induced landslides require a certain amount of water to fall, infiltrate, and accumulate in the ground for landslides to occur (Campbell, 1975; Baum et al., 2010; Bogaard and Greco, 2016), and for the majority of the rainy hours in the study period the rainfall infiltration and accumulation processes were insufficient to trigger landslides. For the remaining hours

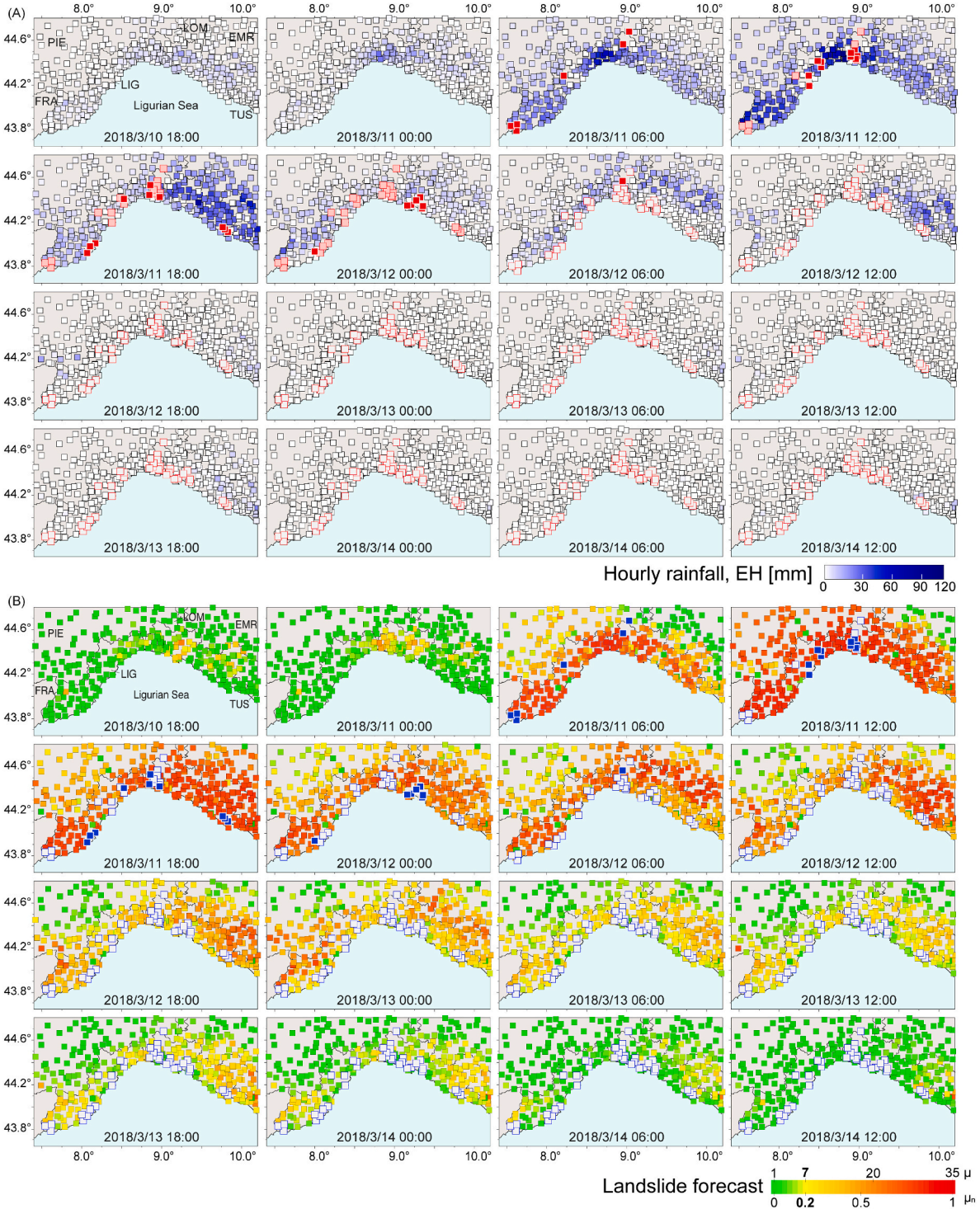

Fig. 8. Rainfall measurements and landslide forecasts from 10 March 18:00 to 14 March 18:00, 2018, in the Liguria region and the neighbouring areas, NW Italy, for 383 rain gauges. (A) Cumulated rainfall in six-hour periods. (B) Landslide occurrence probability every six hours. Rain gauges (squares, from green to yellow to red) show $\mu_n = \mu/35$, the forecasted hourly landslide occurrence probability. In (A) and (B), black squares show rain gauges with nearby landslides reported in the 6-h period, and grey squares rain gauges with nearby landslides reported in the preceding periods. See Fig. 1F for location of Liguria region.

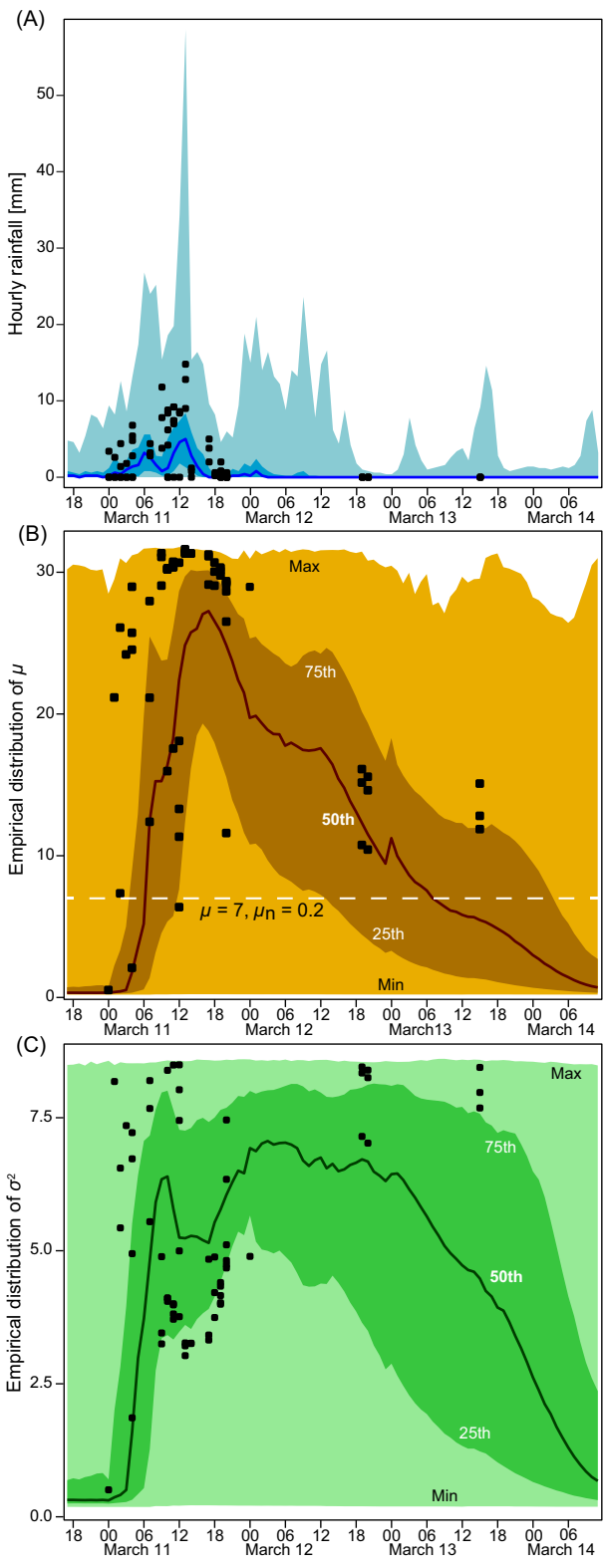

Fig. 9. Rainfall measurements and landslide forecasts from 10 March 18:00 to 14 March 18:00, 2018, in the Liguria region and the neighbouring areas, NW Italy, for the 383 rain gauges shown in Fig. 8. Charts show 50th percentile (thick lines), interquartile range, 25–75th percentiles (darker colours), and min-max range (lighter colours). Black squares are reported landslides. (A) Hourly rainfall measurements. (B) Mean of PBD, μ. Grey dashed line shows $\mu = 7$. (C) Variance of PBD, σ^2. See Fig. 1F for location of Liguria region.

(18.81 %), $\mu_n \geq 0.2$ – *i.e.*, 7 or more forecasters agreed on the prediction of landslide occurrence. Also, of the 184,080 h covered by the diachronic analysis, 98.62 % have at least one rain gauge with $\mu_n \geq 0.2$ confirming the empirical evidence that rain-induced landslides are common in Italy (Calvello and Pecoraro, 2018; Peruccacci et al., 2023). The evidence that almost all rain gauges are associated with at least one landslide confirms that the rain gauge network is sufficient to predict rain-induced landslides in Italy (Mondini et al., 2023).

Further analysis of the "forecast mat" (Figs. 10) reveals temporal and spatial differences in the frequency, f of hours with $\mu_n \geq 0.2$, with annual variations from 21.22 % in 2010 and 20.85 % in 2014 to 13.74 % in 2022 and 12.64 % in 2006 (Fig. 10D), and geographical variations from Campania (19.71 %) and Lazio (18.96 %) with the highest frequency, to Liguria (15.37 %) and Veneto (14.53 %) (Fig. 10G). Overall, the spatial and temporal variations depend on where and when the landscape was forced by rainfall during the two-decade period 2002–2022 and on different propensities of the landscape to generate landslides *i.e.*, variations in landslide susceptibility (Chung and Fabbri, 1999; Guzzetti et al., 2005; Reichenbach et al., 2018) that we do not consider in this work.

Exploiting an independent set, $\{\Omega\}$ of 1916 landslides in the ITALICA catalogue (Peruccacci et al., 2023) characterised by different geographical (λ) and temporal (κ) uncertainties and not used to Train-Validate-Test the deep networks and for the system demonstration (Fig. 7), we perform an independent evaluation of the "forecast mat". We first check the hourly forecasts at all the rain gauges within 10 km of the landslides in the period when the slope failures were reported – from 2 to 24 h, depending on the temporal accuracy of the landslide, κ. We expect that where and when landslides have been reported in set $\{\Omega\}$, the forecasts at the nearby rain gauges are $\mu \geq 7$ *i.e.*, seven or more forecasters (deep networks) agree on the prediction of possible landslide occurrence based on the local rainfall history, r. Fig. 12 A shows that for the majority of the 1916 landslides in the $\{\Omega\}$ set, 88.31 % have $\mu \geq 7$ and about half (49.95 %) have $\mu \geq 29$ – *i.e.*, almost all the forecasters agree in predicting their occurrence. These are true positives (TP). Only 11.79 % of the landslides have $\mu < 7$. These are false negatives (FN). Due to the incompleteness of the landslide information, we cannot know the true negatives (TN) and false positives (FP); a known problem in the landslide literature (Calvello and Piciullo, 2016; Piciullo et al., 2017). Fig. 12 A also shows that regardless of their spatial (λ) and temporal (κ) accuracy, the relative distributions of the landslide forecasts are all similar, and that most of the landslides with low (λ_{100}) or very low (λ_{300}) geographical accuracy, and with very low (κ_3) temporal accuracy were forecasted correctly by the system. We see this as evidence of the robustness of the system even for landslides with low and very low accuracy not used to construct the deep networks.

Next, we look at the distribution of the individual hourly forecasts when the landslides in the $\{\Omega\}$ set were reported, considering their temporal accuracy, κ. Given the assumed dependence of landslide occurrence on rainfall, and given the inherent variation of the dynamic rainfall fields, we expect the forecasts to be more accurate where the reported landslides are closer to the rain gauges where the forecasts are made *i.e.*, where the measured rainfall is closer to the (unknown) rainfall at the location of the landslide. Fig. 12B shows the dependence of the median values of the hourly forecasts on the distance from the rain gauges for the 53,844 h for which forecasts are available, and does not reveal any evident bias of the predictions with the distance to the landslides. We see this as evidence of the adequacy of the Italian rain gauge network (Fig. 1A) for landslide forecasting over the observation period. Colours in the plot portray nine landslide groups based on the geographical and temporal accuracy of the landslide information, and do not reveal evident biases of the predictions dependent on the accuracy of the landslide information.

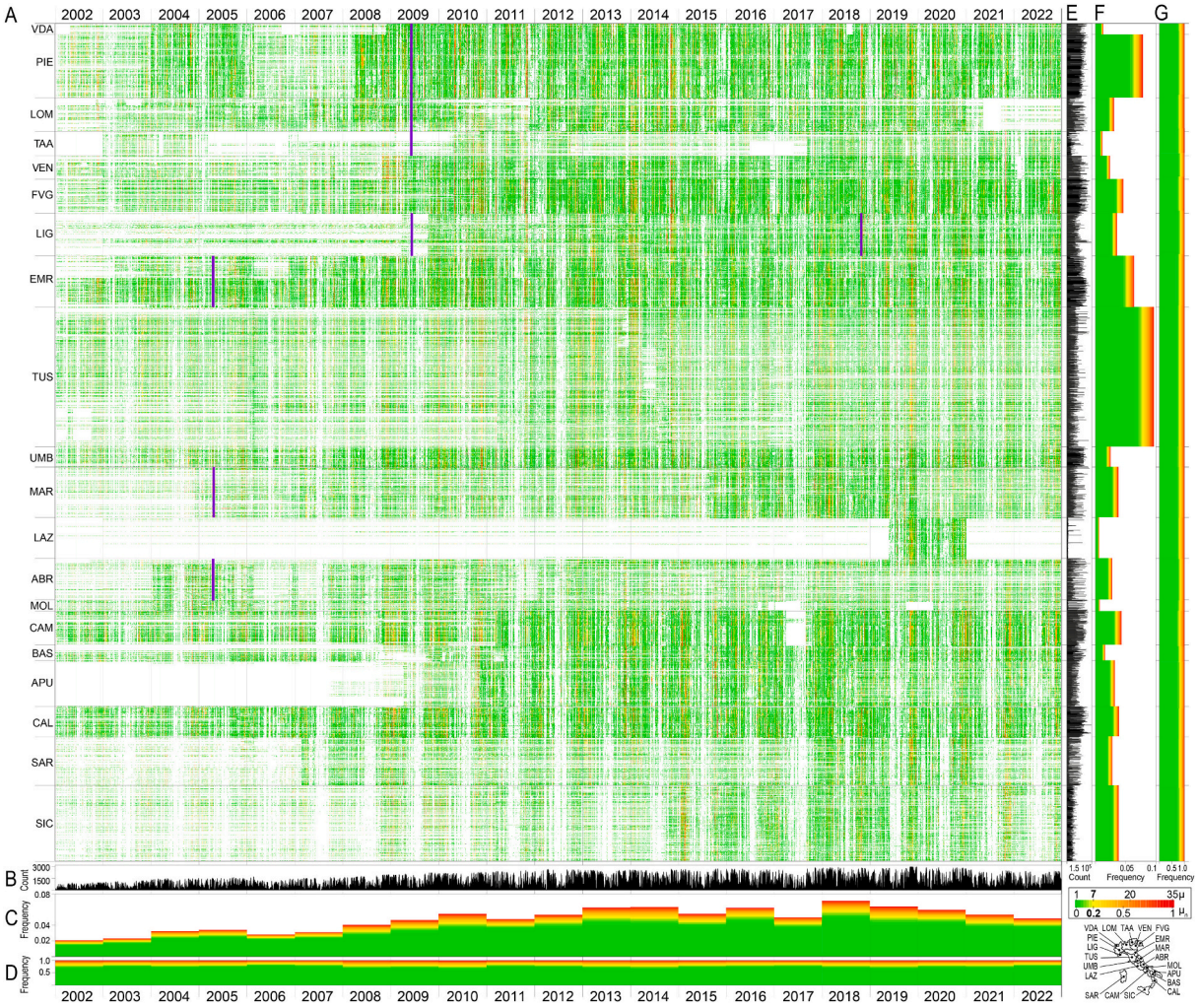

Fig. 10. Long term, diachronic analysis of landslide occurrence probability. (A) "Probability mat" shows landslide occurrence probability, $\mu_n = \mu/35$. x-axis shows time from 1 January 2002 00:00 to 31 December 2022 23:59, and y-axis 4031 rain gauges arranged by Italian region from NW to SE. Pixels, from green to yellow to red, show μ_n, the hourly landslide occurrence probability. Yellow indicates $\mu = 7$, $\mu_n = \mu/35 = 0.2$, the best trade-off in the ROC curve obtained for {Z} (Fig. 7). White pixels show hours without forecasts. Violet bars with Roman numbers show portions of the "mat" portrayed in Fig. 11. Bar charts show (B) count of forecasts per hour; (C) frequency of μ_n, per year; (D) frequency of μ_n in each year; (E) count of hourly forecasts per each rain gauge; (F) frequency of μ_n, per region; and (G) frequency of μ_n in each region. See supplementary materials Tables 3 to 9.

We conclude that the prediction system provides a good spatio-temporal representation of the information on landslide occurrence and associated uncertainty available in the ITALICA catalogue (Peruccacci et al., 2023), and we assume that the "forecast mat" shown in Fig. 12 provides representative information for considerations of the hazard posed by rain-induced landslides in Italy in the two-decade period 2002–2022. We stress that the quantitative information on possible landslide occurrence provided by the "forecast mat" (Figs. 10) is not otherwise available, due to the lack of systematic information on when and where landslides have occurred, a consequence of the inherent incompleteness of the landslide catalogues, in Italy and elsewhere (Kirschbaum Bach et al., 2009; Calvello and Pecoraro, 2018; Peruccacci et al., 2023).

7.4. Hazard assessment

Assuming that the long-term diachronic analysis shown in Fig. 10 is a good estimate of the landslide occurrence probability between 2002 and 2022, and that 21 years is a sufficiently long period for a multi-decade estimate of landslide hazard, we conclude that in the areas where the forecast system has predicted a larger frequency, f of hours when landslides were expected (*i.e.*, $\mu_n \geq 0.2$), landslide hazard was higher than where the system predicted a lower frequency. For each rain gauge in susceptible areas ($S = 1$), Fig. 13 shows the geographical distribution of the frequency of hours in which landslides were expected as deviations from the national mean frequency ($\bar{f} = 17.58$).

Visual inspection of the map reveals significant patterns. The central Alps have a higher frequency than the western and the eastern Alps, with the exception of the Valle d'Aosta (W), the Julian Alps, and Carso (E), which show an opposite trend. The western and central parts of the Liguria region have a lower frequency than the eastern part. Most of the hills and mountains in Emilia-Romagna, in Tuscany and in the Italian peninsula along the Tyrrhenian coast have a higher frequency than along the Adriatic and Ionian coasts. Western and central Sardinia have a higher frequency than the eastern side, and the Tyrrhenian side of Sicily has a higher frequency than the eastern and south-eastern parts. Overall, the patterns in the deviations from the mean frequency are explained by the direction of the prevailing storms, which originate in the Atlantic and move eastwards, hitting the mountain ranges from the west.

Fig. 13 condenses into a single synoptic map the estimated (modelled) relative frequency of landslide occurrence over the two-

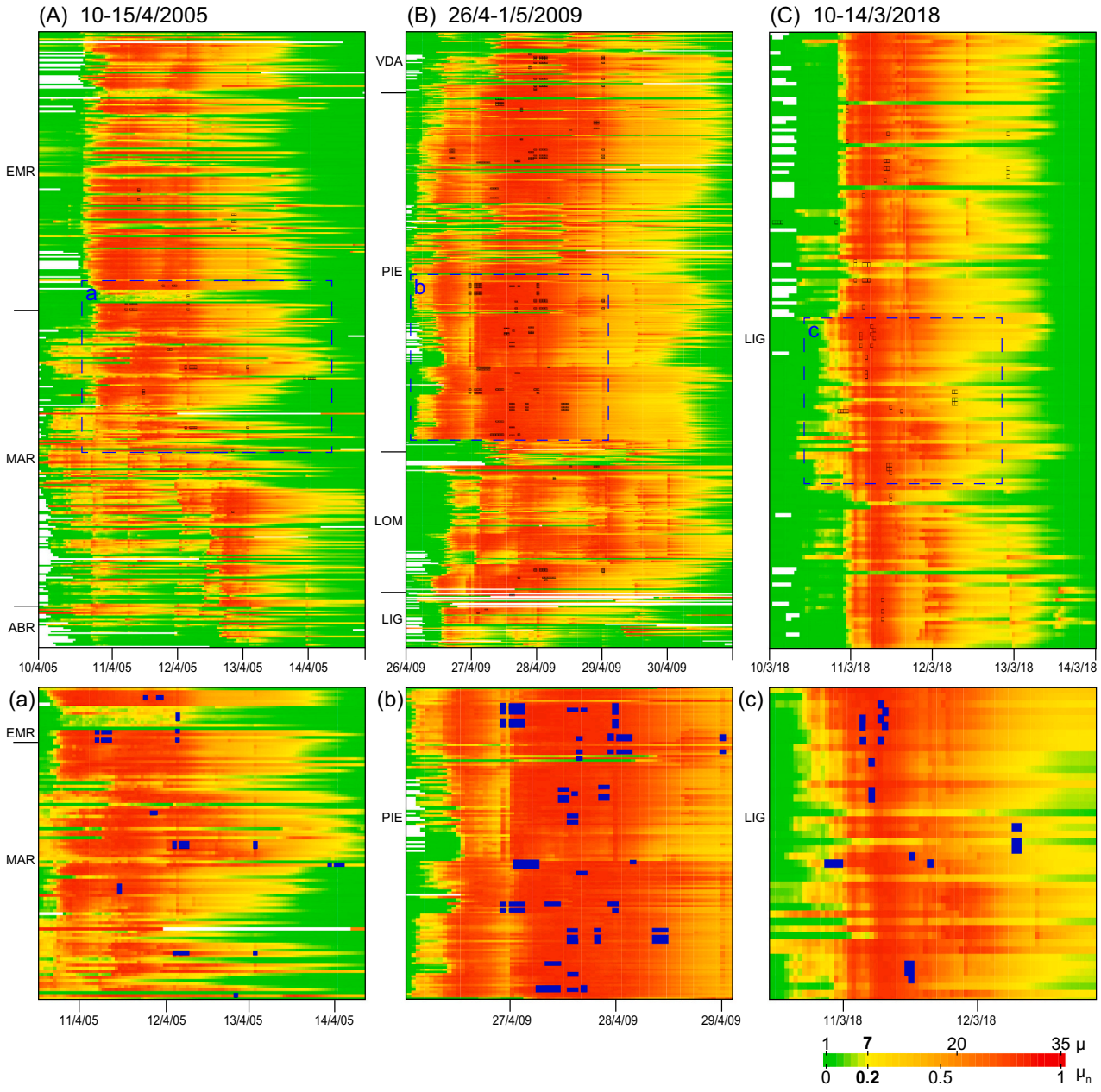

Fig. 11. Rainfall diachronic analysis of landslide occurrence probability for three illustrative periods. (A) 10–15 April 2005 in the Emilia Romagna and Marche regions. (B) 26 April - 1 May 2009 in the Valle d'Aosta, Piedmont, Lombardy and Liguria regions. (C) 10–14 March 2018 in the Liguria region. (a), (b), (c) are enlargements of the main charts. In the "probability mats" each pixel, from green to yellow to red, shows $\mu_n = \mu/35$, the hourly landslide occurrence probability. Yellow indicates $\mu = 7$, $\mu_n = \mu/35 = 0.2$, the best trade-off in the ROC curve obtained for {Z} (Fig. 7). Blue pixels are hours with reported landslides, considering the temporal accuracy of the information. See Fig. 1F for location of Valle d'Aosta, Piedmont, Lombardy and Liguria regions.

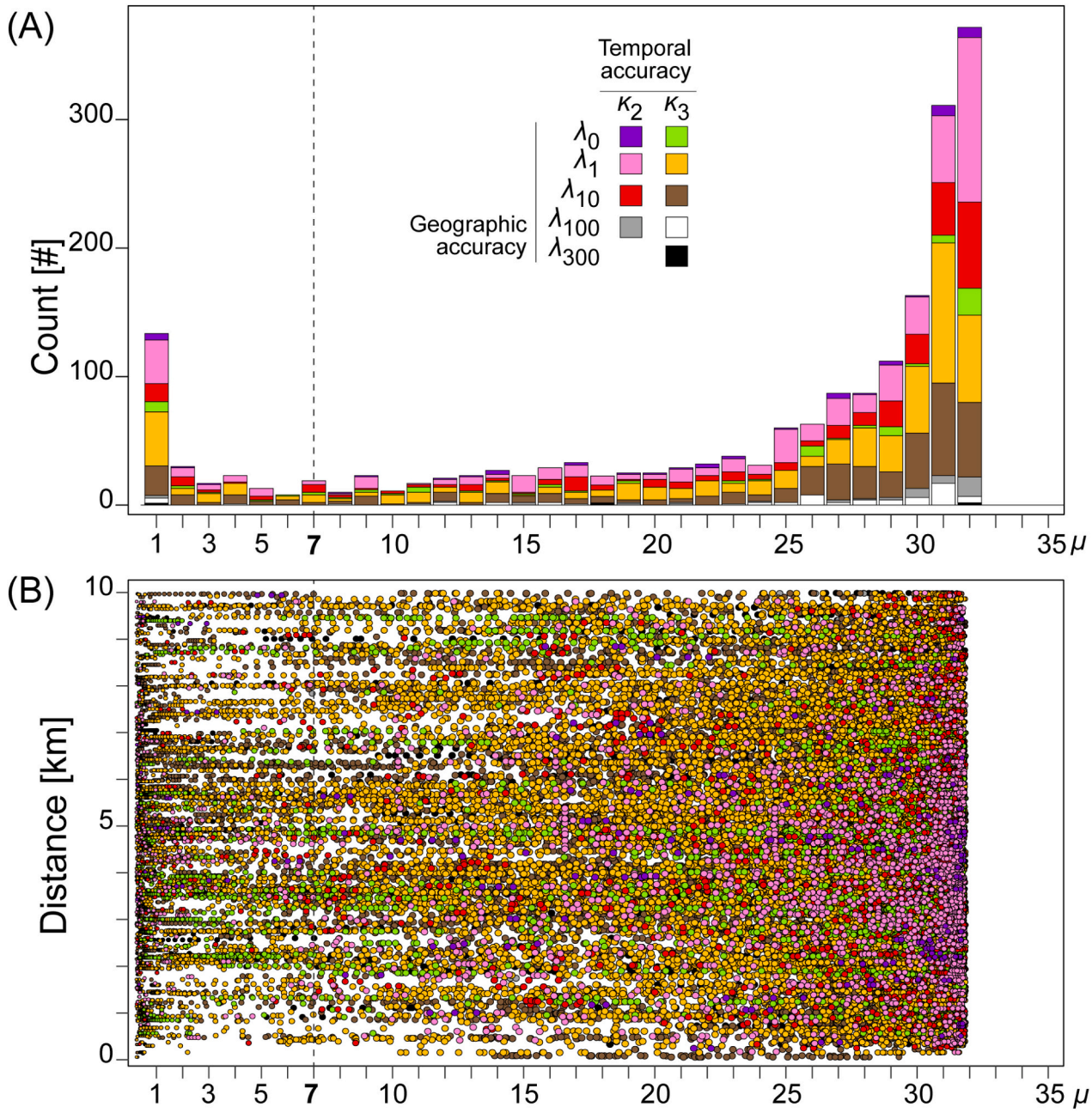

Fig. 12. Analysis of the probabilistic prediction mat shown in Fig. 10 for 1916 landslides in the independent Ω set not used to Train-Validate-Test and demonstrate the forecasting system. (A) Count of landslide occurrence predictions median values. (B) Dependence of the median values of the hourly forecasts (x-axis) on the distance between a reported landslide and the rain gauge used for the predictions (y-axis). In the plots, colours show nine groups based on geographical and temporal accuracy of the landslide information. Geographical accuracy, λ in 5 classes: λ_0, very high accuracy, exact landslide location; λ_1, high accuracy, $\lambda < 1$ km^2; λ_{10}, medium accuracy, $1 \leq \lambda < 10$ km^2; λ_{100}, low accuracy, $10 \leq \lambda < 100$ km^2; λ_{300}, very low accuracy, $100 \leq \lambda < 300$ km^2. Temporal accuracy, κ in two classes: κ_2 when the part of the day is known *e.g.*, early morning, late morning, midday, early afternoon, late afternoon, early night, night; κ_3 when only the day of the landslide is known.

decade period 2002–2022, given the rainfall measured over the same period at 4031 rain gauges. The real frequency remains unknown due to the incompleteness of the landslide information (Calvello and Pecoraro, 2018; Peruccacci et al., 2023), a consequence of the lack of systematic landslide detection and mapping systems (Guzzetti, 2021b). Since rain-induced landslides are ubiquitous in Italy where $S = 1$, we consider the map in Fig. 13 to be a representation of the rain-induced landslide hazard in Italy between 2002 and 2022. We stress that this is new information not available from landslide catalogues (Calvello and Pecoraro, 2018; Peruccacci et al., 2023), inventory maps (Trigila et al., 2010), or synoptic-scale susceptibility zonations (Günther et al., 2014; Loche et al., 2022).

8. Discussion

Synoptic scale, short (hours to a few days) to long (multi-decadal) term spatio-temporal prediction of rain-induced landslides is key for the design and operation of early warning systems, for landslide surveillance over large and very large areas, for modern efforts to mitigate the environmental, economic, and social consequences of landslides, and for

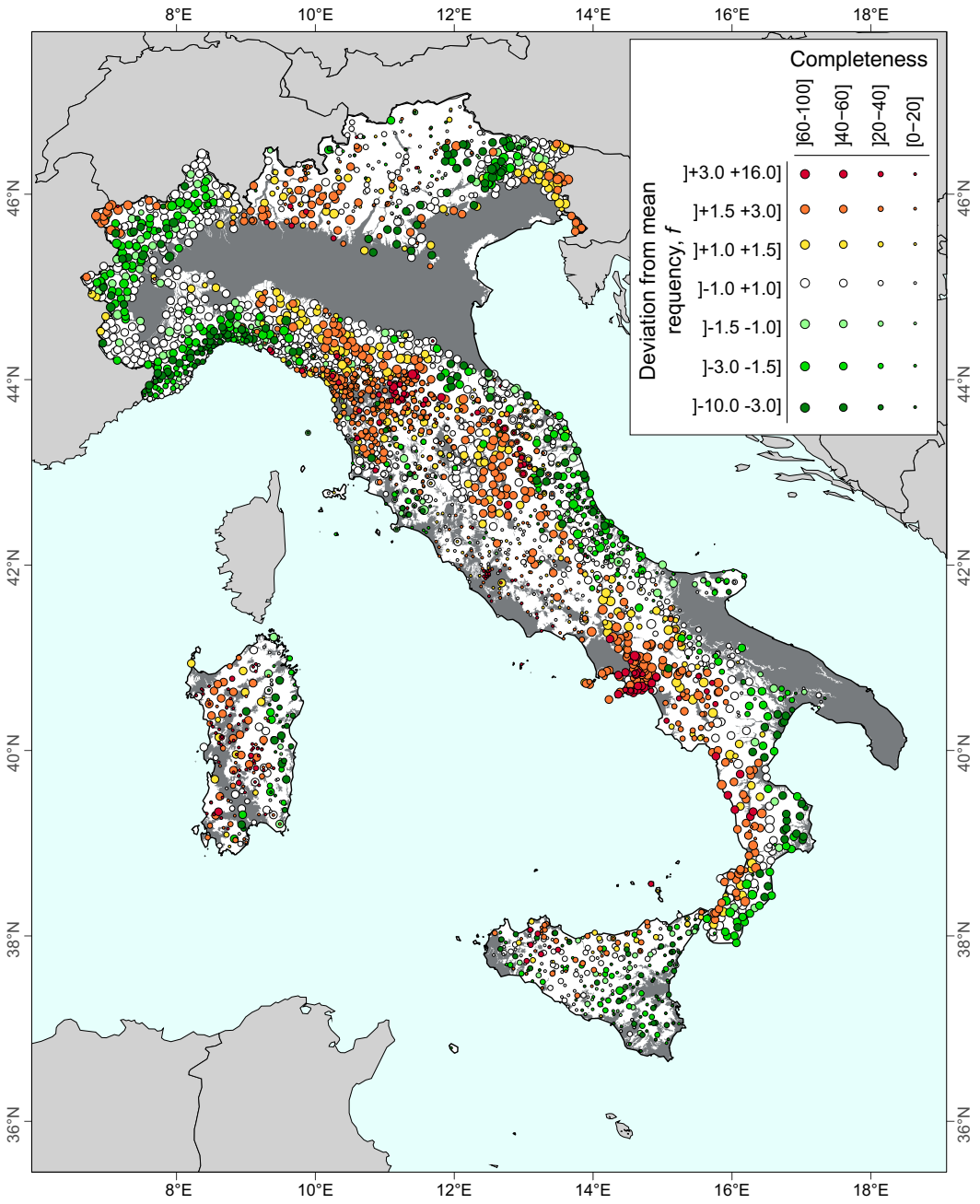

Fig. 13. Frequency of hours when landslides were expected (*i.e.*, where $\mu_n \geq 0.2$) between 2002 and 2022, in Italy. For each rain gauge in susceptible areas (*i.e.*, where $S = 1$), map shows the deviation of the hourly frequency from the national mean frequency, $\bar{f} = 17.58$. The colour of the dots shows the deviation and the size the percentage of hours out of the total number of hours, in four classes. Dark grey areas are non-susceptible areas (Marchesini et al., 2014).

the implementation of effective risk management and adaptation strategies (European Commission Joint Research Centre, 2017). Here, we have proposed a general approach that uses chronicle, events, and technical reports information in an archive inventory (Peruccacci et al., 2023) and hourly rainfall measurements to obtain a probabilistic, synoptic-scale forecast of rain-induced landslides over periods of hours to days. We then used the large set of hourly landslide forecasts to estimate the decadal frequency of rain-induced slope failures, a proxy for long term landslide hazard for timescales of interest for civil protection and environmental adaptation management strategies in a warming climate (Gariano and Guzzetti, 2016; Haque et al., 2019; Pánek, 2019; Intergovernmental Panel on Climate Change, 2021).

Compared to previous work (Mondini et al., 2023), in our experiment we adopted a less physically informed approach to the spatio-temporal modelling of the possible occurrence of rain-induced landslides in Italy. Mondini et al. (2023) assumed that rainfall duration and average rainfall intensity calculated for predetermined rainfall events for different triggering and antecedent periods were responsible for landslide occurrence. Here, we make fewer and less restrictive assumptions about the role of rainfall history in the possible occurrence of landslides, assuming only that the hourly rainfall history in the three days prior to the landslide (variables EH, TR_1, TR_2, …, TR_{71}, TR_{72}), and the antecedent rainfall in the 30 day antecedent period (variable TR_{73-792}), are relevant to the occurrence, or non-occurrence, of landslides. Thus, our approach is more “data driven” and less “physically informed”. Given our limited understanding of the physical processes

controlling landslide initiation at the synoptic scale, the approach makes full use of the information available in rainfall and landslide data and we consider it more appropriate for a data-driven method.

8.1. Short term landslide forecasting

To cope with the uncertainty inherent to the landslide information (Fig. 1A), the rainfall data (Fig. 1D), and our lack of full understanding of the occurrence processes of rain-induced landslides at the synoptic scale, we adopted (i), a stochastic prediction framework in which the possible occurrence of rain-induced landslides is the outcome of a Bernoulli trial – *i.e.*, a random experiment with two possible results, "success" when landslides occur, and "failure" when landslides do not occur and (ii), an ensemble, $\mathscr{M}$ of 35 deep networks (Fig. 5) informed by hourly rainfall measurements and binary information on the occurrence or lack of occurrence of landslides, with associated spatial (λ) and temporal (κ) accuracy.

We tested different geometries for the deep networks and larger ensembles of network models – up to 105 models – and we did not observe significant variations and spread in the modelling results for the Training and the Test-Validation phases, measured by the Train and Validation accuracies and their difference, the Train and Validation losses, Score, the Threshold, G_{mean} score (GMS), Area Under the ROC Curve (A_{ROC}), Balance accuracy (BA), $F1_{score}$, and Cohen's k. We also tested different geometries for the deep networks, and selected the geometry shown in Fig. 5 as a good compromise between performance and overfitting. We acknowledge that using different network geometries and different numbers of deep networks will have changed the modelling results and the system performance. However, we maintain that the results will not have changed significantly.

To cope with the much larger number of hours in the rainfall records without landslides (> 99.9 %) compared to the hours with landslides (< 0.1 %), to train the deep networks (Fig. 5) we used an imbalance ratio of 5 : 1 – *i.e.*, five hours without landslides for every hour with landslides – a compromise between the need to represent the inherent imbalance in the physical process (*e.g.*, landslides do not occur every time it rains) and the limited capacity of the deep networks to deal with highly imbalanced datasets (*e.g.*, He and Garcia, 2009). We tested different imbalance ratios and found that with increasing imbalance the probability calculated for the hourly records with landslides (TP) and for the records without landslides (TN) both decreased slightly, but the overall performance increased because of the very large number of hourly records without landslides. For imbalance ratios larger than 20 : 1, the role of the records with landslides was difficult to interpret.

Following Mondini et al. (2023), we adopted the simplifying assumption that susceptibility can take two values, $S = 1$ where landslides can occur and $S = 0$ elsewhere, and we modelled the possible occurrence of landslides where $S = 1$. This simplification can be relaxed to $0 \leq S \leq 1$ to account for local landslide susceptibility conditions, provided relevant, geographically and temporally distributed environmental information is available to assess susceptibility in probabilistic terms in the periods of the analysis. We contend that this information is difficult to obtain over very large areas (Reichenbach et al., 2018).

We captured the agreement between the 35 forecasters in the ensemble $\mathscr{M}$ – the 35 deep network models – using the PDB (Hoeffding, 1956; Wang, 1993; Biscarri et al., 2018) whose mean, μ and variance, σ^2 are our prediction of landslide occurrence and its uncertainty measure. This is a form of expert elicitation (O'Hagan et al., 2006). To combine the outcomes of the 35 models and their uncertainty, we used the PDB because, by construction, there is stochastic independence between the outcomes of the Bernoulli trials.

Based on the results of the ROC analysis on the independent demonstration subset {Z} (Fig. 6), we selected $\mu_n \geq 0.2$, or $\mu \geq 7$, – *i.e.*, 7 or more (out of 35) forecasters agreed on predicting landslide occurrence – to discriminate the rainfall histories expected to generate landslides. Selection of a different threshold will result in different forecasting scores, and in a different performance of the forecast system. We acknowledge that the prediction accuracy of the single deep network models affects the overall accuracy of the probabilistic and of the "crisp" forecasts. However, we maintain that the use of bagging (Breiman, 1996) and adoption of the PDB to combine the forecasts mitigate the weight of the individual models.

The successful application of the short-term forecast system – measured by the very small Brier scores and the lack of geographical and temporal biases (Fig. 7) – has multiple implications. From an environmental perspective, it is confirmed that in a large and complex landscape where rain-induced landslides are common (Trigila et al., 2010; Calvello and Pecoraro, 2018; Peruccacci et al., 2023), the dynamic rainfall forcing controls the location ("where") and timing ("when") of the landslides during a storm, with consequences for landscape modelling, for estimating the number and size of the triggered landslides (Bellugi et al., 2021), and for predicting the timing and location of rain-triggered landslides (Mondini et al., 2023). The data-driven results further indicate that where slope failures can occur (*i.e.*, where $S = 1$) due to rainfall forcing the transient rainfall history, r controls the location and timing of the slope failures. This is consistent with existing understanding and spatially distributed mechanistic modelling of slope instability forced by rainfall (Baum et al., 2008, 2010; Bogaard and Greco, 2016; Reid et al., 2015; Formetta et al., 2016; Alvioli and Baum, 2016; Bout et al., 2018; Mirus et al., 2025).

From an operational perspective, the result shows that in a diverse landslide-prone landscape forced by rainfall, the rainfall history contains the necessary information to forecast the occurrence probability of rain-induced landslides without the need to establish rainfall thresholds (Guzzetti et al., 2008; Gonzalez, 2024), and to decide *a priori* on a period over which to consider rainfall to divide the precipitation history into events that trigger landslides and those that do not (Melillo et al., 2018). This has consequences for landslide surveillance and early warning (Piciullo et al., 2018; Guzzetti et al., 2020) and it can contribute to regional operational landslide forecasting (Figs. 8, 9).

8.2. Long term landslide prediction and hazard assessment

We obtained the "forecast mat" shown in Fig. 10 by systematically applying our forecasting system to the full set {R} of hourly rainfall data. In the probabilistic "mat", the "warp" (the columns) represents individual hours between 1 January 2002 at 00:00 and 31 December 2022 at 23:59 (local time), and the "weft" (the rows) represents the 4031 rain gauges available to us, loosely arranged from NW to SE. For each grid cell (*i.e.*, for each hour at each rain gauge), the "mat" provides quantitative, information on the agreement between the 35 predictors (*i.e.*, the deep network models) and their variability, given by the PBD mean, μ and variance, σ^2, respectively. The "mat" condenses the $\approx 2.49 \times 10^7$ spatially distributed hourly forecasts in a single, long term (two decades) representation of the modelled probability of landslide occurrence. This is a unique result for Italy, and to the best of our knowledge possibly for the world, that we consider a proxy for landslide hazard (Varnes, 1984; Chung and Fabbri, 1999; Guzzetti et al., 2005) in the two-decade period 2002–2022.

The selection of a specific threshold (*i.e.*, $\mu \geq 7$, $\mu_n = 7/35 \geq 0.2$) – decided by the system performance on the {Z} set (Fig. 6) – has transformed the hourly forecasts from probabilistic to deterministic (*i.e.*, "crisp") potentially facilitating the operational use of the forecasts and the detection of long term patterns of landslide occurrence, or non-occurrence, in the "forecast mat" (Fig. 10), but losing information about the uncertainty of the forecasts. In the individual hourly forecasts, the variance of PBD accounts for the uncertainties inherent in the modelling framework. Operational users can exploit this information to help modulate landslide warnings and advices, and to initiate or terminate risk reduction actions. In the "forecast mat", the long term frequency of "crisp" forecasts aggregates the predictions over a two-

decade period. For such a long period the variance of the hourly forecasts is less relevant as the short term (hourly) variations due to aleatory uncertainty average out, and it becomes more relevant whether the system captures the long term frequency, or the spatial and temporal trends, rather than the uncertainty at any given time and rain gauge. The forecast system is probabilistic for both the short term (hourly, Figs. 8) and the long term (multi-decadal, Figs. 10) predictions, but the interpretation of the uncertainty changes. We acknowledge that how epistemic uncertainty propagates in our multi decadal diachronic analysis is unknown and requires the assumption that our deep network models and parameters are valid over the entire observation period.

Our landslide predictors (*i.e.*, the 35 forecasters) were fully connected deep networks (Fig. 5). However, any other predictor adopting a data-driven, mechanicistic, or a mixed model approach capable of providing probabilistic estimates of landslide occurrence probability for every hour at each rain gauge with an associated uncertainty will do the job. In principle, the framework can cope with any data-driven, statistical, and mechanistic prediction models, or their complex combination, provided that the predictors model independent Bernoulli trials. We consider this an improvement over existing spatio-temporal models of landslide occurrence probability. Other ensembles of probabilistic predictors may require different combination approaches including *e.g.*, Bayesian Model Averaging (Gelman et al., 2013), Hierarchical Bayesian (Congdon, 2019), Mixture Models (Frühwirth-Schnatter, 2006), Logistic Stacking (Bishop, 2006).

To consider the "forecast mat" (Figs. 10) an estimate of the hazard posed by rain-induced landslides in Italy from 2002 to 2022 (Figs. 13) we need to assume uniformitarianism (Lyell, 1875, chapter XIV; Scott, 1963; Haff, 1996; Baker, 2014; Furlani and Ninfo, 2015) *i.e.*, that the physical processes that lead to the occurrence of rain-induced landslides in Italy have not changed – or have not changed significantly – in this period. The meteorological, geomorphological, hydrological, geomechanical, and land use and land cover conditions that led to rain-induced slope failures may have changed locally as a result of climate change, land-use and land-cover changes, the occurrence of other natural events that condition landslide occurrence such as forest fires, earthquakes or permafrost thaw, but these events have not altered the physical mechanisms for triggering landslides. Thus, we maintain that the assumption holds. As mentioned above, we also assume that the deep network models and their parameters have remained valid over the observation period.

8.3. Possible developments

A well-known difficulty in the spatio-temporal prediction of rain-induced landslides over large and very large areas is the lack of multi-temporal information on landslide occurrence. Despite the variety of remote sensing technologies that can accurately detect slope failures over large areas (Mondini et al., 2021; Casagli et al., 2023; Novellino et al., 2024), we expect that the lack of landslide occurrence information will remain a problem in many areas preventing significant progress in spatio-temporal landslide prediction efforts. A related issue is the lack of accurate information on the landslide occurrence time, a key piece of information for relating landslide occurrence to the rainfall history. In our experiment, about 1/3 of the landslides had a temporal accuracy between two and five hours (Fig. 1D). To improve the spatio-temporal prediction models, information on the exact time of occurrence of a larger number of rain-triggered landslides is needed. This information can be obtained *e.g.*, by systematically exploiting existing seismic networks to accurately determine the time or period of occurrence of – at least some –landslide (Ekström and Stark, 2013; Chao et al., 2016, 2017; Manconi and Mondini, 2022). For example, the Swiss Seismological Service records information on mass movements in Switzerland detected by its seismic network with minute accuracy (Service, 2025).

For our experiment we used rainfall measurements taken by a dense network of rain gauges (Fig. 1A) and we made the landslide forecasts at the location of the rain gauges, and not where the landslides have occurred. Although (i) the distance between the landslides and the rain gauges was limited (average $\approx$ 4.49 km, min = 0.03 km, max = 10 km), (ii) the forecasts were good even for the $\{\Omega\}$ set encompassing landslides with lower spatial and temporal accuracy, and (iii) independent research has shown that interpolating the rainfall measurements at the location of the landslides may not necessarily provide better prediction results (Marra, 2019), it may be of interest – and possibly beneficial – to predict landslides where they occur, particularly if $0 \geq S \geq 1$ is considered. This requires accurate spatially and temporally distributed rainfall data available from weather radar networks or precipitation products that combine distributed rainfall estimates obtained from weather radars and point measurements obtained from rain gauges (Ochoa-Rodriguez et al., 2019). The difficulty here lays in the availability of accurate spatially and temporally distributed rainfall data over a sufficiently long period for the empirical relationship between rainfall history and landslide occurrence to be robust.

For the modelling, we used a set of Fully Connected Neural (FCN) networks with a relatively simple five-layer geometry (Fig. 5). Use of different neural network types, including Convolutional Neural Networks (CNN) (LeCun and Bengio, 1995), Long Short-Term Memory (LSTM) networks (Hochreiter and Schmidhuber, 1997), Temporal Convolutional Networks (TCN) (Lea et al., 2017), and Gated Recurrent Units (GRU) network (Chung et al., 2014), may allow for a better characterization of the spatial and temporal evolution of the rainfall driver of landslide occurrence. This may provide better space-time forecasts of landslides triggered by complex rainfall fields. It may also provide better forecasts at the landslide locations. However, use of CNN, LSTM, TCN or GRU network types will not be straightforward as it will require a significant change in the structure of the rainfall and landslide information used to inform the networks. The deep networks should model the Bernoulli trials with adequate cost functions, else, different network aggregation strategies will be required. Use of different deep network types may become justified should high resolution space-time rainfall information (*e.g.*, taken by weather radars) be available for long periods.

We tested our probabilistic prediction approach in Italy, but the approach is general and applicable to any area where similar rainfall and landslide information is available. Rainfall is the most common trigger of landslides (Wieczorek, 1996), but we expect the approach to work for other landslide triggers, including earthquakes and rapid snowmelt, provided sufficient information is available to construct robust prediction models. In principle, the approach is robust to climate, environmental, and societal changes, and to changes in the predictor models. However, the predictors themselves may not be equally robust to the changes. Here, the problem remains the availability of data to build reliable and robust prediction models.

We emphasise that the proposed probabilistic prediction approach has allowed us to address the uncertainty associated with landslide triggering processes across different spatial and temporal scales – from slopes to landscapes, and from hours to decades – and the uncertainty in environmental data and modelling simplifying assumptions (Marzocchi and Jordan, 2014). We argue that formulating a spatio-temporal prediction of landslide occurrence in probabilistic terms across multiple temporal and spatial scales can also allow for the design of scenarios with associated uncertainty, and make landslide prediction comparable and additive to predictions made for other hazards in a multi-hazard framework (Gill and Malamud, 2014, 2016). Finally, we argue that the considerations made on landslide hazard open up the possibility of reconsidering the current approach that interprets hazard as an inherent property of a landscape measured by the joint probability of landslide spatial occurrence, temporal recurrence, and magnitude (Guzzetti et al., 2005), in favour of an alternative approach that considers hazards as a combination of several prediction models, each with a degree of uncertainty.

9. Conclusions

Motivated by the evidence that the dynamically changing rainfall pattern in different geographical and environmental settings controls the onset, location, timing, and frequency of rain-induced landslides, and building on recent modelling results showing that rain-induced landslides can be predicted in space and time using hourly rainfall measurements (Mondini et al., 2023), we proposed a probabilistic modelling framework for synoptic scale, short-term (from hours to days) to long-term (from years to decades) spatio-temporal prediction of rain-induced landslides. To address the biases, gaps, and limitations inherent in the modelling data, as well as the lack of a complete understanding of the landslide triggering processes at the synoptic scale, we constructed an ensemble of 35 deep network models each simulating an independent Bernoulli trial to represent the probability of landslide occurrence, given the rainfall history and information on landslide occurrence in Italy between 2002 and 2022. We combined the outputs of the Bernoulli trials using the Poisson binomial distribution (Hoeffding, 1956; Wang, 1993; Biscarri et al., 2018), a discrete probability distribution whose mean and variance we take to be the expected landslide prediction and its uncertainty. We constructed and demonstrated (Figs. 6 and 7) the forecasting system using information on 3722 landslides and hourly rainfall measurements in the 21-year period from January 2002 to December 2022, in Italy. Then, we applied the system to the full set of 184,080 h in the same period to obtain a long-term representation of the probability of rain-induced landslide occurrence in Italy (Fig. 10).

The experiment confirmed that a Poisson binomial distribution informed by a set of relatively simple deep network models (Fig. 5) was able to forecast the short-term (hourly) probability of landslide occurrence over a large and diverse area such as Italy with high accuracy – measured by very low Brier scores (Brier, 1950) – and no apparent geographical or temporal bias, despite inhomogeneities in the rainfall and the landslide information (Fig. 1), over the 21-year period 2002–2022 (Fig. 10).

From an environmental perspective, the modelling results confirmed that in a large and complex landscape where rain-induced landslides are common – such as Italy (Trigila et al., 2010; Calvello and Pecoraro, 2018; Peruccacci et al., 2023) – the dynamic, transient rainfall forcing controls where and when shallow landslides occur during a rainfall event. This has implications for predicting the time and location of the rain-induced landslides (Mondini et al., 2023), the number and size of the triggered landslides (Bellugi et al., 2021), and for modelling the evolution of landscapes controlled by slope processes. From an operational perspective, we showed that in large diverse landslide-prone landscapes forced by rainfall, the transient precipitation history has the necessary information to forecast the occurrence probability of rain-induced slope failures without the need to establish rainfall thresholds (Guzzetti et al., 2008; Gonzalez, 2024) or to decide *a priori* on a period over which to consider rainfall to divide the precipitation history into events that trigger landslides and those that do not (Melillo et al., 2018). This has implications for landslide surveillance and early warning (Piciullo et al., 2018; Guzzetti et al., 2020), and may contribute to improved geographical operational landslide forecasting.

The application of the forecasting system to the 184,080 h between 1 January 2002 and 31 December 2022 allowed to obtain a multi-decadal representation of the expected long-term occurrence probability of rain-induced landslides (Fig. 10), the analysis of which confirmed that rain-induced slope failures are common in Italy. The evidence that almost all rain gauges were associated with at least one historical landslide in the observation period confirmed that the rain gauge network (Fig. 1D) is adequate to predict rain-induced landslides in Italy. The multi-decadal probabilistic "forecast mat" (Fig. 12) provides unique information on the hazard posed by rain-induced landslides in Italy from 2002 to 2022, an information not otherwise available from landslide catalogues (Calvello and Pecoraro, 2018; Peruccacci et al., 2023), inventory maps (Trigila et al., 2010), or synoptic-scale susceptibility zonations (Günther et al., 2014; Loche et al., 2022). This information may support the design and implementation of long-term landslide adaptation and risk reduction strategies.

Our research has proposed an alternative approach to landslide hazard assessment that considers hazard as the combination of prediction models with their associated uncertainty – in our modelling framework through a Poisson binomial distribution. This opens up the possibility of reconsidering the common approach that interprets hazard as an inherent property of a landscape measured by the joint probability of the spatial occurrence, temporal recurrence, and magnitude of landslides (Guzzetti et al., 2005).

Authors contributions

Alessandro C. Mondini: designed the study, designed the probabilistic framework, constructed the deep networks, analysed and discussed the results, wrote the paper - review & editing. **Fausto Guzzetti:** designed the study, prepared the data, analysed and discussed the results, wrote the paper - review & editing, prepared the figures and the supplementary materials. **Massimo Melillo:** designed the study, prepared the data, analysed and discussed the results, prepared the figures and the supplementary materials. **Antonio Pievatolo:** designed the probabilistic framework, analysed and discussed the results.

Use of trade, product or firm names

In the article, use of trade, product or firm names is for descriptive purposes and does not imply endorsement by the authors or the Italian Consiglio Nazionale delle Ricerche (https://www.cnr.it).

Software and hardware details

The statistical analyses were performed in R 4.3.3 to 4.4.2 (https://www.r-project.org/) with the support of RStudio 2024.04.0 to 2024.12.0 (https://posit.co/products/open-source/rstudio/). The neural network model is written in Tensorflow 2.3.0 (https://www.tensorflow.org/) with the support of Python 3.8 (https://www.python.org/), Keras 1.1.2 (https://keras.io/), Scikit-learn 0.24.1 (https://scikit-learn.org/), Numpy 1.21.2 (https://numpy.org/), and Pandas 1.2.3. (https://pandas.pydata.org) in Ubuntu 20.04 (https://ubuntu.com/).

Declaration of competing interest

The authors declare no competing interests.

Acknowledgments

We thank Mauro Rossi for maintaining the database of rainfall measurements used in the study. In Figs. 1, 8, and 13, geographical boundaries are provided by the European Environment Agency (EEA) and the Italian Istituto Nazionale di Statistica (ISTAT). We thank two anonymous referees for their constructive comments.

Appendix A. List of variables and symbols

Variable, symbol	Description
a	Artificial neuron
c	Dichotomous value of landslide susceptibility, S
f	Frequency of hours in which landslides are expected to occur
$\bar{f}$	National mean of f
h	Sigmoid activation function
p	Value of P
r	Local rainfall history at each rain gauge
l	Outcome of the landslide occurrence Bernoulli trial, $[1, 0]$
$tanh$	Hyperbolic tangent activation function
EH	Cumulative rainfall in the reference hour
L	Landslide occurrence
P	Probability
$P(L\|R,S)$	Probability of landslide occurrence, given a rainfall history, R, and susceptibility, S
$P(L\|R)$	Probability of landslide occurrence, given a rainfall history, R
R	Rainfall history
S	Landslide susceptibility
TR_i	Cumulative rainfall in the i reference preceding period
$\mathscr{M}$	Neural networks ensemble
R	Set of rainfall records used in the study
T	Subset of rainfall records for model testing
V	Subset of rainfall records for model validation
U	Subset of rainfall records for model training
Z	Subset of rainfall records for independent demonstration
T	Transpose
β	Bias added to the weighted input before activation
λ	Geographical accuracy of the ITALICA information
μ	Mean of the Poisson binomial distribution
μ_n	μ rescaled by the number of Bernoulli trials (number of deep networks)
σ^2	Variance of the Poisson binomial distribution
θ	Weight of the connections betweens neurons
κ	Temporal accuracy of the ITALICA information
Ω	Independent set of landslides used to evaluate the probabilistic prediction mat

Appendix B. List of abbreviations and acronyms

Abbreviation	Description
A_{ROC}	Area under the Receiver operating characteristic curve
AA	Alpine-Appenine Transition Zone topographic province
AB	Adriatic Borderline topographic province
AL	Alpine Mountain System topographic province
AP	Appenine Mountain System province province
BS	Brier Score
BSk	Cold semiarid climate
CHIRPS	Climate Hazards Centre Infrared Precipitations with Stations
Cfa	Humid subtropical climate
Csa	Hot-summer Mediterranean climate
CNN	Convolutional Neural Network
Dfb	Warm-summer humid continental climate
ECDF	Empirical Cumulative Distribution Function
ET	Cold climate
$F1_{score}$	Harmonic mean of precision and recall
Cohen κ	Cohen's kappa coefficient
FCN	Fully Connected neural Network
FN	False Negative
FP	False Positive
FPR	False Positive Rate
GMS	G_{mean} Score
GRU	Gated Recurrent Units
ITALICA	ITAlian rainfall-induced LandslIdes CAtalogue
LEWS	Landslide Early Warning System
LSTM	Long-Short Term Memory
MAP	Mean annual precipitation
PBD	Poisson binomial distribution
PMF	Probability Mass Function
ROC	Receiver operating characteristic curve
SA	Sardinia topographic province
SI	Sicily topographic province
TB	Thyrrenian topographic province
TCN	Temporal Convolutional Network
TN	True Negative
TP	True Positive
TPR	True Positive Rate

Appendix C. Supplementary data

Supplementary data to this article can be found online at https://doi.org/10.1016/j.scitotenv.2025.179453.

Data availability

Landslide data used in the study is available from Zenodo, https://doi.org/10.5281/zenodo.8009366. Rainfall data are the property of the regional governments of Italy and should be obtained from them.

References

Abadi, M., Agarwal, A., Barham, P., Brevdo, E., Chen, Z., Citro, C., Corrado, G.S., Davis, A., Dean, J., Devin, M., Ghemawat, S., Goodfellow, I., Harp, A., Irving, G., Isard, M., Jia, Y., Jozefowicz, R., Kaiser, L., Kudlur, M., Levenberg, J., Mané, D., Monga, R., Moore, S., Murray, D., Olah, C., Schuster, M., Shlens, J., Steiner, B., Sutskever, I., Talwar, K., Tucker, P., Vanhoucke, V., Vasudevan, V., Viégas, F., Vinyals, O., Warden, P., Wattenberg, M., Wicke, M., Yu, Y., Zheng, X., 2015. TensorFlow: Large-Scale Machine Learning on Heterogeneous Systems. https://doi.org/10.5281/zenodo.4724125 (Last accessed on 2024-12-29).

Aggarwal, C., 2018. Neural Networks and Deep Learning: A Textbook. Springer International Publishing. https://doi.org/10.1007/978-3-319-94463-0.

Aleotti, P., 2004. A warning system for rainfall-induced shallow failures. Eng. Geol. 73, 247–265. https://doi.org/10.1016/j.enggeo.2004.01.007.

Alvioli, M., Baum, R.L., 2016. Parallelization of the TRIGRS model for rainfall-induced landslides using the message passing interface. Environ. Model. Softw. 81, 122–135. https://doi.org/10.1016/j.envsoft.2016.04.002.

Alvioli, M., Marchesini, I., Reichenbach, P., Rossi, M., Ardizzone, F., Fiorucci, F., Guzzetti, F., 2016. Automatic delineation of geomorphological slope units with r.slopeunits v1.0 and their optimization for landslide susceptibility modeling. Geosci. Model Dev. 9, 3975–3991. https://doi.org/10.5194/gmd-9-3975-2016.

Anagnostopoulos, G.G., Fatichi, S., Burlando, P., 2015. An advanced process-based distributed model for the investigation of rainfall-induced landslides: the effect of process representation and boundary conditions. Water Resour. Res. 51, 7501–7523. https://doi.org/10.1002/2015WR016909.

Baker, V.R., 2014. Uniformitarianism, earth system science, and geology. Anthropocene 5, 76–79. https://doi.org/10.1016/j.ancene.2014.09.001.

Bandis, S.C., Delmonaco, G., Dutto, F., Margottini, C., Mortara, G., Serafini, S., Trocciola, A., 1999. Landslides and Precipitaton: The Event of 4-6th November 1994 in the Piedomont Region, North Italy. In: Casale, R., Margottini, C. (Eds.), Floods and Landslides: Integrated Risk Assessment. Springer-Verlag Berlin Heidelberg, pp. 315–326. https://doi.org/10.1007/978-3-642-58609-5_20. Environmental Science.

Basu, S., Dassios, A., 2002. A cox process with log-normal intensity. Insurance: mathematics and economics 31, 297–302. https://doi.org/10.1016/S0167-6687(02)00152-X.

Baum, R.L., Savage, W.Z., Godt, J.W., 2008. TRIGRS— a Fortran program for transient rainfall infiltration and grid-based regional slope-stability analysis, version 2.0. Open-file Report 2008–1159. U.S. Geological Survey. https://pubs.usgs.gov/of/2008/1159/downloads/pdf/OF08-1159.pdf.

Baum, R.L., Godt, J.W., Savage, W.Z., 2010. Estimating the timing and location of shallow rainfall-induced landslides using a model for transient, unsaturated infiltration. J. Geophys. Res. 115, F03013. https://doi.org/10.1029/2009JF001321.

Beck, H.E., McVicar, T.R., Vergopolan, N., Berg, A., Lutsko, N.J., Dufour, A., Zeng, Z., Jiang, X., van Dijk, A.I.J.M., Miralles, D.G., 2023. High-resolution (1 km) Köppen-Geiger maps for 1901–2099 based on constrained CMIP6 projections. Scientific Data 10, 724. https://doi.org/10.1038/s41597-023-02549-6.

Bellugi, D.G., Milledge, D.G., Cuffey, K.M., Dietrich, W.E., Larsen, L.G., 2021. Controls on the size distributions of shallow landslides. Proc. Natl. Acad. Sci. 118, e2021855118. https://doi.org/10.1073/pnas.2021855118.

Benz, S.A., Blum, P., 2019. Global detection of rainfall-triggered landslide clusters. Nat. Hazards Earth Syst. Sci. 19, 1433–1444. https://doi.org/10.5194/nhess-19-1433-2019.

Berti, M., Pizziolo, M., Scaroni, M., Generali, M., Critelli, V., Mulas, M., Tondo, M., Lelli, F., Fabbiani, C., Ronchetti, F., Ciccarese, G., Dal Seno, N., Ioriatti, E., Rani, R., Zuccarini, A., Simonelli, T., Corsini, A., 2025. RER2023: the landslide inventory dataset of the May 2023 Emilia-Romagna meteorological event. Earth System Science Data 17, 1055–1074. https://doi.org/10.5194/essd-17-1055-2025.

Bessette-Kirton, E.K., Cerovski-Darriau, C., Schulz, W.H., Coe, J.A., Kean, J.W., Godt, J.W., Thomas, M.A., Hughes, K.S., 2019. Landslides triggered by hurricane Maria: assessment of an extreme event in Puerto Rico. GSA Today 29, 4–10. https://doi.org/10.1130/GSATG383A.1.

Bianchi, C., Salvati, P., 2025. Rapporto Periodico sul Rischio posto alla Popolazione Italiana da Frane e da Inondazioni - Anno 2024. Technical Report. CNR, Istituto di Ricerca per la Protezione Idrogeologica. https://doi.org/10.30437/REPORT2024.

Biscarri, W., Zhao, S.D., Brunner, R.J., 2018. A simple and fast method for computing the poisson binomial distribution function. Computational Statistics & Data Analysis 122, 92–100. https://doi.org/10.1016/j.csda.2018.01.007.

Bishop, C.M., 2006. Pattern Recognition and Machine Learning. Springer, New York. https://www.springer.com/gp/book/9780387310732.

Bogaard, T.A., Greco, R., 2016. Landslide hydrology: from hydrology to pore pressure. WIREs Water 3, 439–459. https://doi.org/10.1002/wat2.1126.

Borga, M., Dalla Fontana, G., Da Ros, D., Marchi, L., 1998. Shallow landslide hazard assessment using a physically based model and digital elevation data. Environ. Geol. 35, 81–88. https://doi.org/10.1007/s002540050295.

Bout, B., Lombardo, L., van Westen, C., Jetten, V., 2018. Integration of two-phase solid fluid equations in a catchment model for flashfloods, debris flows and shallow slope failures. Environ. Model Softw. 105, 1–16. https://doi.org/10.1016/j.envsoft.2018.03.017.

Brabb, E.E., 1984. Innovative approaches to landslide Hazard and risk mapping innovation dans la preparation des Cartes de glissements. In: Proceedings of the IV International Symposium on Landslides, Toronto, Canada, pp. 307–324.

Brabb, E.E., 1985. Innovative approaches to landslide hazard and risk mapping. In: International Landslide Symposium Proceedings. Canada, Toronto, pp. 17–22.

Breiman, L., 1996. Bagging predictors. Mach. Learn. 24, 123–140. https://doi.org/10.1007/BF00058655.

Brier, G.W., 1950. Verification of forecasts expressed in terms of probability. Mon. Weather Rev. 1, 1–3. https://doi.org/10.1175/1520-0493(1950)078%3C0001:VOFEIT%3E2.0.CO;2.

Burton, A., Bathurst, J.C., 1998. Physically based modelling of shallow landslide sediment yield at a catchment scale. Environ. Geol. 35, 89–99. https://doi.org/10.1007/s002540050296.

Calvello, M., Pecoraro, G., 2018. FraneItalia: a catalog of recent Italian landslides. Geoenviron. Disasters 5. https://doi.org/10.1186/s40677-018-0105-5.

Calvello, M., Piciullo, L., 2016. Assessing the performance of regional landslide early warning models: the edumap method. Nat. Hazards Earth Syst. Sci. 16, 103–122. https://doi.org/10.5194/nhess-16-103-2016.

Campbell, R.H., 1975. Soil Slips, Debris Flows, and Rainstorms in the Santa Monica Mountains and Vicinity, Southern California, vol. 51. U.S. Geological Survey, Washington, D.C. https://pubs.usgs.gov/pp/0851/report.pdf.

Carrara, A., 1983. Multivariate models for landslide hazard evaluation. J. Int. Assoc. Math. Geol. 15, 403–426. https://doi.org/10.1007/BF01031290.

Casagli, N., Intrieri, E., Tofani, V., Gigli, G., Raspini, F., 2023. Landslide detection, monitoring and prediction with remote-sensing techniques. Nature Reviews Earth & Environment 4, 51–64. https://doi.org/10.1038/s43017-022-00373-x.

Chan, R.K.S., Pang, P.L.R., Pun, W.K., 2003. Recent Developments in the Landslip Warning System in Hong Kong, in: Proceedings of the 14th Southeast Asian Geotechnical Conference. Balkema Publisher, Lisse, The Netherlands, pp. 141–147.

Chao, W.A., Zhao, L., Chen, S.C., Wu, Y.M., Chen, C.H., Huang, H.H., 2016. Seismology-based early identification of dam-formation landquake events. Sci. Rep. 6, 19259. https://doi.org/10.1038/srep19259.

Chao, W.A., Wu, Y.M., Zhao, L., Chen, H., Chen, Y.G., Chang, Jui-Ming, Lin, Che-Min, 2017. A first near real-time seismology-based landquake monitoring system. Sci. Rep. 7, 43510. https://doi.org/10.1038/srep43510.

Choi, K.Y., Cheung, R.W.M., 2013. Landslide disaster prevention and mitigation through works in Hong Kong. J. Rock Mech. Geotech. Eng. 5, 354–365. https://doi.org/10.1016/j.jrmge.2013.07.007.

Chung, C.J.F., Fabbri, A.G., 1999. Probabilistic prediction models for landslide Hazard mapping. Journal of Photogrammetry and Remote Sensing 65, 1389–1399.

Chung, J., Gulcehre, C., Cho, K., Bengio, Y., 2014. Empirical Evaluation of Gated Recurrent Neural Networks on Sequence Modeling.

Coe, J.A., Winchell, M., Crovelli, R.A., Savage, W.Z., 2000. Preliminary map showing landslide densities, mean recurrence intervals, and exceedance probabilities as determined from historic records, Seattle, Washington. United States Geological Survey Open File Report 00–303.

Congdon, P.D., 2019. Bayesian Hierarchical Models: With Applications Using R, Second ed. CRC Press, Boca Raton, FL https://www.routledge.com/Bayesian-Hierarchical-Models-With-Applications-Using-R-Second-Edition/Congdon/p/book/9781498785754.

Crosta, G.B., 1998. Regionalization of rainfall thresholds: an aid to landslide hazard evaluation. Environ. Geol. 35, 131–145. https://doi.org/10.1007/s002540050300.

Crosta, G.B., Frattini, P., 2000. Rainfall thresholds for triggering soil slips and debris flows. In: Mediterranean Storms 2000 - Proceedings Second EGS Plinius Conference, Siena, Italy, pp. 463–487. October 2000.

Crovelli, R., Coe, J., 2009. Probabilistic estimation of numbers and costs of future landslides in the San Francisco Bay region. Georisk 3, 206–223.

Crozier, M.J., 1999. Prediction of rainfall-triggered landslides: a test of the antecedent water status model. Earth Surf. Process. Landf. 24, 825–833. https://doi.org/10.1002/(SICI)1096-9837(199908)24:9<825::AID-ESP14>3.0.CO;2-M.

Dahal, A., Lombardo, L., 2025. Towards physics-informed neural networks for landslide prediction. Eng. Geol. 344, 1–14. https://doi.org/10.1016/j.enggeo.2024.107852.

Dahal, A., Huser, R., Lombardo, L., 2024a. At the junction between deep learning and statistics of extremes: formalizing the landslide Hazard definition. Journal of Geophysical Research: Machine Learning and Computation 1, e2024JH000164. https://doi.org/10.1029/2024JH000164.

Dahal, A., Tanyas, H., van Westen, C., van der Meijde, M., Mai, P.M., Huser, R., Lombardo, L., 2024b. Space–time landslide hazard modeling via ensemble neural networks. Nat. Hazards Earth Syst. Sci. 24, 823–845. https://doi.org/10.5194/nhess-24-823-2024.

Dietrich, W.E., Wilson, C.J., Montgomery, D.R., McKean, J., 1993. Analysis of erosion thresholds, channel networks, and landscape morphology using a digital terrain model. J. Geol. 101, 259–278. https://doi.org/10.1086/648220.

Diggle, P.J., Moraga, P., Rowlingson, B., Taylor, B.M., et al., 2013. Spatial and spatio-temporal log-Gaussian cox processes: extending the geostatistical paradigm. Stat. Sci. 28, 542–563.

Donnini, M., Santangelo, M., Gariano, S.L., Bucci, F., Peruccacci, S., Alvioli, M., Althuwaynee, O., Ardizzone, F., Bianchi, C., Bornaetxea, T., Brunetti, M.T., Cardinali, M., Esposito, G., Grita, S., Marchesini, I., Melillo, M., Salvati, P., Yazdani, M., Fiorucci, F., 2023. Landslides triggered by an extraordinary rainfall event in Central Italy on September 15, 2022. Landslides 20, 2199–2211. https://doi.org/10.1007/s10346-023-02109-4.

Ekström, G., Stark, C.P., 2013. Simple scaling of catastrophic landslide dynamics. Science 339, 1416–1419. https://doi.org/10.1126/science.1232887.

Emberson, R., Kirschbaum, D., Stanley, T., 2020. New global characterisation of landslide exposure. Nat. Hazards Earth Syst. Sci. 20, 3413–3424. https://doi.org/10.5194/nhess-20-3413-2020.

Emberson, R., Kirschbaum, D.B., Amatya, P., Tanyas, H., Marc, O., 2022. Insights from the topographic characteristics of a large global catalog of rainfall-induced landslide event inventories. Nat. Hazards Earth Syst. Sci. 22, 1129–1149. https://doi.org/10.5194/nhess-22-1129-2022.

European Commission Joint Research Centre, 2017. Science for Disaster Risk Management 2017: Knowing Better and Losing Less, 2017 ed. Publications Office European Commission, Joint Research Centre, LU. https://doi.org/10.2788/842809.

Fang, Z., Wang, Y., van Westen, C., Lombardo, L., 2024. Landslide hazard spatiotemporal prediction based on data-driven models: estimating where, when and how large landslide may be. Int. J. Appl. Earth Obs. Geoinf. 126, 103631. https://doi.org/10.1016/j.jag.2023.103631.

Formetta, G., Rago, V., Capparelli, G., Rigon, R., Muto, F., Versace, P., 2014. Integrated physically based system for modeling landslide susceptibility. Procedia Earth and Planetary Science 9, 74–82. https://doi.org/10.1016/j.proeps.2014.06.006.

Formetta, G., Simoni, S., Godt, J.W., Lu, N., Rigon, R., 2016. Geomorphological control on variably saturated hillslope hydrology and slope instability. Water Resour. Res. 52, 4590–4607. https://doi.org/10.1002/2015WR017626.

Frühwirth-Schnatter, S., 2006. Finite mixture and Markov switching models. Springer, New York. https://doi.org/10.1007/978-0-387-35768-3.

Funk, C., Peterson, P., Landsfeld, M., Pedreros, D., Verdin, J., Shukla, S., Husak, G., Rowland, J., Harrison, L., Hoell, A., Michaelsen, J., 2015. The climate hazards infrared precipitation with stations—a new environmental record for monitoring extremes. Scientific Data 2, 150066. https://doi.org/10.1038/sdata.2015.66.

Furlani, S., Ninfo, A., 2015. Is the present the key to the future? Earth Sci. Rev. 142, 38–46. https://doi.org/10.1016/j.earscirev.2014.12.005.

Gariano, S.L., Guzzetti, F., 2016. Landslides in a changing climate. Earth Sci. Rev. 162, 227–252. https://doi.org/10.1016/j.earscirev.2016.08.011.

Gelman, A., Carlin, J.B., Stern, H.S., Dunson, D.B., Vehtari, A., Rubin, D.B., 2013. Bayesian Data Analysis, 3rd ed. Chapman and Hall/CRC, Boca Raton, Florida https://stat.columbia.edu/~gelman/book/.

Gill, J.C., Malamud, B.D., 2014. Reviewing and visualizing the interactions of natural hazards. Rev. Geophys. 52, 680–722. https://doi.org/10.1002/2013rg000445.

Gill, J.C., Malamud, B.D., 2016. Hazard interactions and interaction networks (cascades) within multi-hazard methodologies. Earth Syst. Dynam. 7, 659–679. https://doi.org/10.5194/esd-7-659-2016.

Glade, T., Crozier, M., Smith, P., 2000. Applying probability determination to refine landslide-triggering rainfall thresholds using an empirical "antecedent daily rainfall model". Pure Appl. Geophys. 157, 1059–1079. https://doi.org/10.1007/s000240050017.

Gonzalez, F.C.G., do Carmo Reis Cavacanti, M., Nahas Ribeiro, W., de Mendonça, M.B., Haddad, A.N., 2024. A systematic review on rainfall thresholds for landslides occurrence. Heliyon 10, e23247. https://doi.org/10.1016/j.heliyon.2023.e23247.

Günther, A., Van Den Eeckhaut, M., Malet, J.P., Reichenbach, P., Hervás, J., 2014. Climate-physiographically differentiated Pan-European landslide susceptibility assessment using spatial multi-criteria evaluation and transnational landslide information. Geomorphology 224, 69–85. https://doi.org/10.1016/j.geomorph.2014.07.011.

Guzzetti, F., 2021a. Invited perspectives: landslide populations – can they be predicted? Nat. Hazards Earth Syst. Sci. 21, 1467–1471. https://doi.org/10.5194/nhess-21-1467-2021.

Guzzetti, F., 2021b. On the prediction of landslides and their consequences. In: Sassa, K., Mikoš, M., Sassa, S., Bobrowsky, P.T., Takara, K., dang, K. (Eds.), Understanding and Reducing Landslide Disaster Risk: Volume 1 Sendai Landslide Partnerships and Kyoto Landslide Commitment, 1 ed. vol. 1. Springer international publishing, Cham, pp. 3–32. https://doi.org/10.1007/978-3-030-60196-6_1.

Guzzetti, F., Reichenbach, P., 1994. Towards a definition of topographic divisions for Italy. Geomorphology 11, 57–74. https://doi.org/10.1016/0169-555X(94)90042-6.

Guzzetti, F., Carrara, A., Cardinali, M., Reichenbach, P., 1999. Landslide Hazard evaluation: a review of current techniques and their application in a multi-scale study, Central Italy. Geomorphology 31, 181–216. https://doi.org/10.1016/S0169-555X(99)00078-1.

Guzzetti, F., Reichenbach, P., Cardinali, M., Ardizzone, F., Galli, M., 2003. The impact of landslides in the Umbria region, Central Italy. Nat. Hazards Earth Syst. Sci. 3, 469–486. https://doi.org/10.5194/nhess-3-469-2003.

Guzzetti, F., Cardinali, M., Reichenbach, P., Cipolla, F., Sebastiani, C., Galli, M., Salvati, P., 2004. Landslides triggered by the 23 November 2000 rainfall event in the Imperia Province, Western Liguria, Italy. Eng. Geol. 73, 229–245. https://doi.org/10.1016/j.enggeo.2004.01.006.

Guzzetti, F., Reichenbach, P., Cardinali, M., Galli, M., Ardizzone, F., 2005. Probabilistic landslide hazard assessment at the basin scale. Geomorphology 72, 272–299. https://doi.org/10.1016/j.geomorph.2005.06.002.

Guzzetti, F., Peruccacci, S., Rossi, M., Stark, C.P., 2007. Rainfall thresholds for the initiation of landslides in central and southern Europe. Meteorog. Atmos. Phys. 98, 239–267. https://doi.org/10.1007/s00703-007-0262-7.

Guzzetti, F., Peruccacci, S., Rossi, M., Stark, C.P., 2008. The rainfall intensity - duration control of shallow landslides and debris flows: an update. Landslides 5, 3–17. https://doi.org/10.1007/s10346-007-0112-1.

Guzzetti, F., Ardizzone, F., Cardinali, M., Rossi, M., Valigi, D., 2009. Landslide volumes and landslide mobilization rates in Umbria, Central Italy. Earth Planet. Sci. Lett. 279, 222–229. https://doi.org/10.1016/j.epsl.2009.01.005.

Guzzetti, F., Mondini, A.C., Cardinali, M., Fiorucci, F., Santangelo, M., Chang, K.T., 2012. Landslide inventory maps: new tools for an old problem. Earth Sci. Rev. 112, 42–66. https://doi.org/10.1016/j.earscirev.2012.02.001.

Guzzetti, F., Gariano, S.L., Peruccacci, S., Brunetti, M.T., Marchesini, I., Rossi, M., Melillo, M., 2020. Geographical landslide early warning systems. Earth Sci. Rev. 200, 102973. https://doi.org/10.1016/j.earscirev.2019.102973.

Guzzetti, F., Melillo, M., Mondini, A.C., 2024. Landslide predictions through combined rainfall threshold models. Landslides. https://doi.org/10.1007/s10346-024-02340-7.

Haff, P.K., 1996. 14 limitations on predictive modeling in geomorphology. In: Rhoads, B. L., Thorn, C.E. (Eds.), The Scientific Nature of Geomorphology: Proceedings of the 27th Binghamton Symposium in Geomorphology Held 27–29 September 1996, vol. 1. John Wiley & Sons Ltd, pp. 337–358.

Handwerger, A.L., Fielding, E.J., Huang, M.H., Bennett, G.L., Liang, C., Schulz, W.H., 2019. Widespread initiation, reactivation, and acceleration of landslides in the northern California coast ranges due to extreme rainfall. J. Geophys. Res. Earth 124, 1782–1797. https://doi.org/10.1029/2019JF005035.

Hansen, A., 1984. Landslide hazard analysis. In: Brunsden, D., Prior, D.B. (Eds.), Slope Instability. Wiley & Sons, New York, NY, pp. 523–602.

Haque, U., da Silva, P.F., Devoli, G., Pilz, J., Zhao, B., Khaloua, A., Wilopo, W., Andersen, P., Lu, P., Lee, J., Yamamoto, T., Keellings, D., Wu, J.H., Glass, G.E., 2019. The human cost of global warming: deadly landslides and their triggers (1995–2014). Sci. Total Environ. 682, 673–684. https://doi.org/10.1016/j.scitotenv.2019.03.415.

Haykin, S., 2009. Neural Networks and Learning Machines. Pearson International Edition, Pearson. https://books.google.it/books?id=KCwWOAAACAAJ.

He, H., Garcia, E.A., 2009. Learning from imbalanced data sets. IEEE. https://doi.org/10.1007/978-3-319-98074-4.

Hochreiter, S., Schmidhuber, J., 1997. Long short-term memory. Neural Comput. 9, 1735–1780. https://doi.org/10.1162/neco.1997.9.8.1735.

Hoeffding, W., 1956. On the distribution of the number of successes in independent trials. Ann. Math. Stat. 27, 713–721. https://doi.org/10.1214/aoms/1177728178.

Hubert, M., 1976. Le cartographie en France des Zones Exposées à des Risques liés aux Mouvements du Sol. Cartes ZERMOS. International Association Enginnering Geology Bulletin 16, 80–82. https://doi.org/10.1007/BF02591455.

Intergovernmental Panel on Climate Change, 2021. Climate change 2021: the physical science basis. Cambridge University Press. https://doi.org/10.1017/9781009157896.

Istituto Superiore per la Protezione e la Ricerca Ambientale, 2025. Idrogeo. https://idrogeo.isprambiente.it/ (Last accessed on 2025-02-08).

Jakob, M., 2022. Chapter 14 - landslides in a changing climate. In: Davies, T., Rosser, N., Shroder, J. (Eds.), landslide hazards, risks, and disasters, 2 edition, Hazards and disasters series. Elsevier, pp. 505–579. https://doi.org/10.1016/B978-0-12-818464-6.00003-2.

Jones, J.N., Boulton, S.J., Stokes, M., Bennett, G.L., Whitworth, M.R.Z., 2021. 30-year record of Himalaya mass-wasting reveals landscape perturbations by extreme events. Nat. Commun. 12, 6701. https://doi.org/10.1038/s41467-021-26964-8.

Keefer, D.K., Wilson, R.C., Mark, R.K., Brabb, E.E., Brown, W.M., Ellen, S.D., Harp, E.L., Wieczorek, G.F., Alger, C.S., Zatkin, R.S., 1987. Real-time landslide warning during heavy rainfall. Science 238, 921–925. https://doi.org/10.1126/science.238.4829.921.

Kidd, C., Becker, A., Huffman, G.J., Muller, C.L., Joe, P., Skofronick-Jackson, G., Kirschbaum Bach, D., 2017. So, how much of the earth's surface is covered by rain gauges? Bull. Am. Meteorol. Soc. 98, 69–78. https://doi.org/10.1175/BAMS-D-14-00283.1.

Kirschbaum Bach, D., Adler, R.F., Hong, Y., Hill, S., Lerner-Lam, A., 2009. A global landslide catalog for hazard applications: method, results, and limitations. Nat. Hazards 52, 561–575. https://doi.org/10.1007/s11069-009-9401-4.

Ko, F.W., Lo, F.L., 2018. From landslide susceptibility to landslide frequency: a territory–wide study in Hong Kong. Eng. Geol. 242, 12–22. https://doi.org/10.1016/j.enggeo.2018.05.001.

Kong, V.W.W., Kwan, J.S.H., Pun, W.K., 2020. Hong Kong's landslip warning system–40 years of progress. Landslides 17, 1453–1463. https://doi.org/10.1007/s10346-020-01379-6.

Kuhn, M., Johnson, K., 2013. Applied predictive modeling. Springer. https://doi.org/10.1007/978-1-4614-6849-3.

Lanni, C., McDonnell, J., Hopp, L., Rigon, R., 2013. Simulated effect of soil depth and bedrock topography on near-surface hydrologic response and slope stability. Earth Surf. Process. Landf. 38, 146–159. https://doi.org/10.1002/esp.3267.

Lea, C., Flynn, M.D., Vidal, R., Reiter, A., Hager, G.D., 2017. Temporal convolutional networks for action segmentation and detection. In: Proceedings of the IEEE Conference on Computer Vision and Pattern Recognition (CVPR), pp. 156–165. https://doi.org/10.1109/CVPR.2017.20.

LeCun, Y., Bengio, Y., 1995. Convolutional Networks for Images, Speech, and Time Series, in: Arbib, M. (Ed.). MIT Press, The Handbook of Brain Theory and Neural Networks, p. 1995.
Lim, J., Santinelli, G., Dahal, A., Vrieling, A., Lombardo, L., 2024. An ensemble neural network approach for space–time landslide predictive modelling. Int. J. Appl. Earth Obs. Geoinf. 132, 104037. https://doi.org/10.1016/j.jag.2024.104037.
Lips, E.W., Wieczorek, G.F., 1990. Recurrence of Debris Flows on an Alluvial Fan in Central Utah, in: French, R. (Ed.). Proceedings of the International Symposium Hydraulic/Hydrology of Arid Lands, American Society of Civil Engineers, pp. 555–560.
Loche, M., Alvioli, M., Marchesini, I., Bakka, H., Lombardo, L., 2022. Landslide susceptibility maps of Italy: lesson learnt from dealing with multiple landslide types and the uneven spatial distribution of the national inventory. Earth Sci. Rev. 104125. https://doi.org/10.1016/j.earscirev.2022.104125.
Lombardo, L., Opitz, T., Ardizzone, F., Guzzetti, F., Huser, R., 2020. Space-time landslide predictive modelling. Earth Sci. Rev. 209, 103318. https://doi.org/10.1016/j.earscirev.2020.103318.
Luino, F., 1999. The flood and landslide event of November 4–6 1994 in Piedmont region (northwestern Italy): causes and related effects in Tanaro Valley. Phys. Chem. Earth Solid Earth Geod. 24, 123–129. https://doi.org/10.1016/s1464-1895(99)00007-1.
Lyell, C., 1875. Principles of Geology, 12th ed. 1. John Murray, London.
Manconi, A., Mondini, A.C., 2022. The AlpArray working group. Landslides caught on seismic networks and satellite radars. Nat. Hazards Earth Syst. Sci. 22, 1655–1664. https://doi.org/10.5194/nhess-22-1655-2022.
Marchesini, I., Ardizzone, F., Alvioli, M., Rossi, M., Guzzetti, F., 2014. Non-susceptible landslide areas in Italy and in the Mediterranean region. Nat. Hazards Earth Syst. Sci. 14, 2215–2231. https://doi.org/10.5194/nhess-14-2215-2014.
Marra, F., 2019. Rainfall thresholds for landslide occurrence: systematic underestimation using coarse temporal resolution data. Nat. Hazards 95, 883–890. https://doi.org/10.1007/s11069-018-3508-4.
Marzocchi, W., Jordan, T.H., 2014. Testing for ontological errors in probabilistic forecasting models of natural systems. Proc. Natl. Acad. Sci. 111, 11973–11978. https://doi.org/10.1073/pnas.1410183111.
Melillo, M., Brunetti, M.T., Peruccacci, S., Gariano, S.L., Roccati, A., Guzzetti, F., 2018. A tool for the automatic calculation of rainfall thresholds for landslide occurrence. Environ. Model Softw. 105, 230–243. https://doi.org/10.1016/j.envsoft.2018.03.024.
Michie, D., Spiegelhalter, D.J., Taylor, C.C., 1994. Machine Learning, Neural and Statistical Classification. Ellis Horwood.
Mirus, B.B., Bogaard, T., Greco, R., Stähli, M., 2025. Invited perspectives: integrating hydrologic information into the next generation of landslide early warning systems. Nat. Hazards Earth Syst. Sci. 25, 169–182. https://doi.org/10.5194/nhess-25-169-2025.
Møller, J., Syversveen, A.R., Waagepetersen, R.P., 1998. Log Gaussian cox processes. Scand. J. Stat. 25, 451–482. https://doi.org/10.1111/1467-9469.00115.
Mondini, A.C., Guzzetti, F., Chang, K.T., Monserrat, O., Martha, T.R., Manconi, A., 2021. Landslide failures detection and mapping using synthetic aperture radar: past, present and future. Earth Sci. Rev. 216, 103574. https://doi.org/10.1016/j.earscirev.2021.103574.
Mondini, A.C., Guzzetti, F., Melillo, M., 2023. Deep learning forecast of rainfall-induced shallow landslides. Nature. Communications 14, 2466. https://doi.org/10.1038/s41467-023-38135-y.
Monte, N., Bucci, F., Mevoli, F.A., Santangelo, M., Reichenbach, P., Di Matteo, L., Marchesini, I., 2024. A dataset of geotechnical parameters based on international literature to characterise lithotypes in Italy. Scientific Data 11, 1371. https://doi.org/10.1038/s41597-024-04095-1.
Montgomery, D.R., Dietrich, W.E., 1994. A physically based model for the topographic control on shallow landsliding. Water Resour. Res. 30, 1153–1171. https://doi.org/10.1029/93WR02979.
Moreno, M., Lombardo, L., Crespi, A., Zellner, P.J., Mair, V., Pittore, M., van Westen, C., Steger, S., 2024. Space-time data-driven modeling of precipitation-induced shallow landslides in South Tyrol, Italy. Sci. Total Environ. 912, 169166. https://doi.org/10.1016/j.scitotenv.2023.169166.
Neuland, H., 1976. A prediction model of landslips. CATENA 3, 215–230. https://doi.org/10.1016/0341-8162(76)90011-4.
Nocentini, N., Rosi, A., Piciullo, L., Liu, Z., Segoni, S., Fanti, R., 2024. Regional-scale spatiotemporal landslide probability assessment through machine learning and potential applications for operational warning systems: a case study in Kvam (Norway). Landslides 1–19. https://doi.org/10.1007/s10346-024-02287-9.
Novellino, A., Pennington, C., Leeming, K., Taylor, S., Alvarez, I.G., McAllister, E., Arnhardt, C., Winson, A., 2024. Mapping landslides from space: a review. Landslides 21, 1041–1052. https://doi.org/10.1007/s10346-024-02215-x.
Ochoa-Rodriguez, S., Wang, L.P., Willems, P., Onof, C., 2019. A review of radar-rain gauge data merging methods and their potential for urban hydrological applications. Water Resour. Res. 55, 6356–6391. https://doi.org/10.1029/2018WR023332.
O'Hagan, A., Buck, C.E., Daneshkhah, A., Eiser, J.R., Garthwaite, P.H., Jenkinson, D.J., Oakley, J.E., Rakow, T., 2006. Uncertain Judgements: Eliciting Experts' Probabilities. Wiley, Chichester, UK. https://doi.org/10.1002/0470033312.
Okimura, T., Ichikawa, R., 1985. Prediction method for surface failures by movements of infiltrated water in a surface soil layer. Natural Disaster Sciene 7, 41–51.
Ozturk, U., Bozzolan, E., Holcombe, E.A., Shukla, R., Pianosi, F., Wagener, T., 2022. How climate change and unplanned urban sprawl bring more landslides. Nature 608, 262–265. https://doi.org/10.1038/d41586-022-02141-9.
Pánek, T., 2019. Landslides and quaternary climate changes—the state of the art. Earth Sci. Rev. 196, 102871. https://doi.org/10.1016/j.earscirev.2019.05.015.
Papastathopoulos, I., Tawn, J.A., 2013. Extended generalised Pareto models for tail estimation. Journal of Statistical Planning and Inference 143, 131–143. https://doi.org/10.1016/j.jspi.2012.07.001.
Peres, D.J., Cancelliere, A., 2021. Comparing methods for determining landslide early warning thresholds: potential use of non-triggering rainfall for locations with scarce landslide data availability. Landslides 18, 3135–3147. https://doi.org/10.1007/s10346-021-01704-7.
Perkins, J.P., Oakley, N.S., Collins, B.D., Corbett, S.C., Burgess, W.P., 2024. Characterizing the scale of regional landslide triggering from storm hydrometeorology. EGUsphere 2024, 1–32. https://doi.org/10.5194/egusphere-2024-873.
Peruccacci, S., Brunetti, M.T., Gariano, S.L., Melillo, M., Rossi, M., Guzzetti, F., 2017. Rainfall thresholds for possible landslide occurrence in Italy. Geomorphology 290, 39–57. https://doi.org/10.1016/j.geomorph.2017.03.031.
Peruccacci, S., Gariano, S.L., Melillo, M., Solimano, M., Guzzetti, F., Brunetti, M.T., 2023. The ITAlian rainfall-induced LandslIdes CAtalogue, an extensive and accurate spatio-temporal catalogue of rainfall-induced landslides in Italy. Earth System Science Data 2863–2877. https://doi.org/10.5194/essd-15-2863-2023.
Piciullo, L., Gariano, S.L., Melillo, M., Brunetti, M.T., Peruccacci, S., Guzzetti, F., Calvello, M., 2017. Definition and performance of a threshold-based regional early warning model for rainfall-induced landslides. Landslides 14, 995–1008. https://doi.org/10.1007/s10346-016-0750-2.
Piciullo, L., Calvello, M., Cepeda, J.M., 2018. Territorial early warning systems for rainfall-induced landslides. Earth Sci. Rev. 179, 228–247. https://doi.org/10.1016/j.earscirev.2018.02.013.
Pizziolo, M., Bernardi, M., Daniele, G., Generali, M., Piacentini, D., 2015. In: Lollino, G., Manconi, A., Guzzetti, F., Culshaw, M., Bobrowsky, P., Luino, F. (Eds.), Engineering Geology for Society and Territory -, 5. Springer International Publishing, Cham, pp. 777–780. https://doi.org/10.1007/978-3-319-09048-1_151.
Reichenbach, P., Cardinali, M., De Vita, P., Guzzetti, F., 1998. Regional hydrological thresholds for landslides and floods in the Tiber River basin (Central Italy). Environ. Geol. 35, 146–159. https://doi.org/10.1007/s002540050301.
Reichenbach, P., Rossi, M., Malamud, B.D., Mihir, M., Guzzetti, F., 2018. A review of statistically-based landslide susceptibility models. Earth Sci. Rev. 180, 60–91. https://doi.org/10.1016/j.earscirev.2018.03.001.
Reid, M.E., Christian, S.B., Brien, D.L., Henderson, S.T., 2015. Scoops3D— Software to Analyze Three-Dimensional Slope Stability throughout a Digital Landscape. Technical Report 14-A1.. U.S. Geological Survey. https://doi.org/10.3133/tm14A1.
Roccati, A., Faccini, F., Luino, F., Turconi, L., Guzzetti, F., 2018. Rainfall events with shallow landslides in the Entella catchment, Liguria, northern Italy. Nat. Hazards Earth Syst. Sci. 18, 2367–2386. https://doi.org/10.5194/nhess-18-2367-2018.
Rossi, M., Witt, A., Guzzetti, F., Malamud, B.D., Peruccacci, S., 2010. Analysis of historical landslide time series in the Emilia–Romagna region, northern Italy. Earth Surf. Process. Landf. 35, 1123–1137. https://doi.org/10.1002/esp.1858.
Rossi, M., Guzzetti, F., Salvati, P., Donnini, M., Napolitano, E., Bianchi, C., 2019. A predictive model of societal landslide risk in Italy. Earth Sci. Rev. 196, 102849. https://doi.org/10.1016/j.earscirev.2019.04.021.
Saito, H., Nakayama, D., Matsuyama, H., 2010. Relationship between the initiation of a shallow landslide and rainfall intensity—duration thresholds in Japan. Geomorphology 118, 167–175. https://doi.org/10.1016/j.geomorph.2009.12.016.
Samia, J., Temme, A.J., Bregt, A., Wallinga, J., Guzzetti, F., Ardizzone, F., Rossi, M., 2017. Do landslides follow landslides? Insights in path dependency from a multi-temporal landslide inventory. Landslides 14, 547–558. https://doi.org/10.1007/s10346-016-0739-x.
Santangelo, M., Althuwaynee, O., Alvioli, M., Ardizzone, F., Bianchi, C., Bornaetxea, T., Brunetti, M.T., Bucci, F., Cardinali, M., Donnini, M., Esposito, G., Gariano, S.L., Grita, S., Marchesini, I., Melillo, M., Peruccacci, S., Salvati, P., Yazdani, M., Fiorucci, F., 2023. Inventory of landslides triggered by an extreme rainfall event in Marche-Umbria, Italy, on 15 September 2022. Scientific Data 10, 427. https://doi.org/10.1038/s41597-023-02336-3.
Scott, G.H., 1963. Uniformitarianism, the uniformity of nature, and paleoecology. J. Geol. Geophys. 6, 510–527. https://doi.org/10.1080/00288306.1963.10420063.
Segoni, S., Rosi, A., Rossi, G., Catani, F., Casagli, N., 2014. Analysing the relationship between rainfalls and landslides to define a mosaic of triggering thresholds for regional-scale warning systems. Nat. Hazards Earth Syst. Sci. 14, 2637–2648. https://doi.org/10.5194/nhess-14-2637-2014.
Segoni, S., Lagomarsino, D., Fanti, R., Moretti, S., Casagli, N., 2015. Integration of rainfall thresholds and susceptibility maps in the Emilia Romagna (Italy) regional-scale landslide warning system. Landslides 12, 773–785. https://doi.org/10.1007/s10346-014-0502-0.
Segoni, S., Piciullo, L., Gariano, S.L., 2018. A review of the recent literature on rainfall thresholds for landslide occurrence. Landslides 1–19. https://doi.org/10.1007/s10346-018-0966-4.
Service, S.S, 2025. Sed switzerland mass movements. http://www.seismo.ethz.ch/en/earthquakes/switzerland/massmovements/. Last accessed on 2025-01-31.
Staley, D.M., Kean, J.W., Rengers, F.K., 2020. The recurrence interval of post-fire debris-flow generating rainfall in the southwestern United States. Geomorphology 370, 107392. https://doi.org/10.1016/j.geomorph.2020.107392.
Stanley, T.A., Kirschbaum, D.B., Benz, G., Emberson, R.A., Amatya, P.M., Medwedeff, W., Clark, M.K., 2021. Data-driven landslide Nowcasting at the global scale. Frontiers Earth Sci. 9, 640043. https://doi.org/10.3389/feart.2021.640043.
Trigila, A., Iadanza, C., Spizzichino, D., 2010. Quality assessment of the Italian landslide inventory using GIS processing. Landslides 7, 455–470. https://doi.org/10.1007/s10346-010-0213-0.

Van Asch, T.W., Hendriks, M., Hessel, R., Rappange, F., 1996. Hydrological triggering conditions of landslides in varved clays in the French Alps. Eng. Geol. 42, 239–251. https://doi.org/10.1016/0013-7952(95)00082-8.

van den Bout, B., van Asch, T., Hu, W., Tang, C.X., Mavrouli, O., Jetten, V.G., van Westen, C.J., 2021. Towards a model for structured mass movements: the OpenLISEM hazard model 2.0a. Geosci. Model Dev. 14, 1841–1864. https://doi.org/10.5194/gmd-14-1841-2021.

Van Westen, C., Van Asch, T.W., Soeters, R., 2006. Landslide hazard and risk zonation – why is it still so difficult? Bull. Eng. Geol. Environ. 65, 167–184. https://doi.org/10.1007/s10064-005-0023-0.

van Westen, C., Castellanos, E., Kuriakose, S., 2008. Spatial data for landslide susceptibility, hazard, and vulnerability assessment: an overview. Eng. Geol. 102, 112–131. https://doi.org/10.1016/j.enggeo.2008.03.010.

Varnes, D.J., 1984. International Association of Engineering Geology. In: Landslide Hazard Zonation–A Review of Principles and Practice. UNESCO, Paris, Paris.

Wang, Y.H., 1993. On the number of successes in independedn trials. Stat. Sin. 3, 295–312. http://www.jstor.org/stable/24304959.

Wieczorek, G.F., 1996. Landslide triggering mechanisms, vol. 4. Transportation Research Board, Washington, D.C, pp. 76–90. Number 247 in special Report.

Wilson, R.C., 2012. The rise and fall of a debris-flow warning system for the San Francisco Bay region, California. In: Glade, T., Anderson, M., Crozier, M.J. (Eds.), landslide Hazard and risk. John Wiley & Sons, ltd, Chichester, West Sussex, England, pp. 493–516. https://doi.org/10.1002/9780470012659.ch17.

Witt, A., Malamud, B.D., Rossi, M., Guzzetti, F., Peruccacci, S., 2010. Temporal correlations and clustering of landslides. Earth Surf. Process. Landf. 35, 1138–1156. https://doi.org/10.1002/esp.1998.

Wong, A.C.W., Ting, S.M., Shiu, Y.K., Ho, K.K.S., 2014. Latest developments of Hong Kong's landslip warning system. In: Sassa, K., Canuti, P., Yin, Y. (Eds.), Landslide Science for a Safer Geoenvironment. Springer International Publishing, Cham, pp. 613–618. https://doi.org/10.1007/978-3-319-05050-8_95.